UNIVERSIDADE DE SÃO PAULO

INSTITUTO DE FÍSICA
CAIXA POSTAL 20516
01498 - SÃO PAULO - SP
BRASIL

PUBLICAÇÕES

IFUSP/P-792

SAM REVISITED: ABSORPTIVE UNIFORM SEMI-CLASSICAL APPROXIMATION AND APPLICATION TO HEAVY-ION ELASTIC SCATTERING

M.P. Pato and **M.S. Hussein**
Instituto de Física, Universidade de São Paulo

Junho/1989

SAM REVISITED: ABSORPTIVE UNIFORM SEMICLASSICAL APPROXIMATION AND APPLICATION TO HEAVY-ION ELASTIC SCATTERING

M.P. Pato and **M.S. Hussein***

Instituto de Física, Universidade de São Paulo
C.P. 20516, 01498 São Paulo, SP, Brazil

This paper is dedicated to the memory of W.E. Frahn, a colleague and friend.

*Supported in part by the CNPq.

June – 1989

CONTENTS

1. Introduction
2. The Near–Far, Diffraction–Refraction Decomposition of the Scattering Amplitude
3. Phase Space Equations, Symbols and the Refraction Amplitude
4. Eikonal Representation of the Uniform Semiclassical Absorption–Free Amplitude
5. Applications
6. Conclusions

References

Appendix A – Cubic Rainbow

Appendix B – Relation of the Phase Shift to the Parameters of the Optical Potential

ABSTRACT

The Uniform Semiclassical Approximation is modified to take into account absorption. Symbol calculus and pseudodifferential operators techniques are employed for the purpose. The resulting theory, very similar to the one developed by Frahn and Gross permits the decomposition of the near–side and far–side amplitudes into diffractive and refractive components. Application to several heavy–ion systems at intermediate energies is made.

I. INTRODUCTION

In recent years the elastic scattering of heavy ions has received renewed interest both experimentally and theoretically. This stems principally from the availability of higher energy heavy ion beams which makes possible the study of the ion–ion interaction at shorter distances. One of the most conspicuous manifestation of the probing of short distances in the system is the occurrence of a nuclear rainbow. This effect is connected with the internal branch of the deflection function $\Theta = 2\frac{d\delta(\ell)}{d\ell}$, where $\delta(\ell)$ is the total (Coulomb + nuclear) phase shift. A minimum in this branch at θ_r (at negative angles) would naturally divide the angular space into the dark side, $\theta > \theta_r$ and the illuminated side $\theta < \theta_r$. At angles smaller than θ_r, the angular distribution would, under ideal situations, exhibit Airy oscillations, followed, at $\theta > \theta_r$ by an almost exponential drop.

The presence of strong absorption in the low–ℓ partial waves, considerably modifies the above picture. The contribution of the inner branch of the nuclear deflection function in the rainbow region is strongly damped. Accordingly the Airy oscillations are expected to be washed out. Nevertheless a remmant of the rainbow will be seen in the cross section. The analysis of the elastic scattering data at intermediate energies would then supply invaluable information about the deflection function at negative angles and correspondingly the underlying ion–ion potential. The most spetacular case of a nuclear rainbow is the one "seen" in α–scattering from medium mass nuclei.

The common procedure usually employed in the analysis of the elastic scattering data is the optical model and/or the coupled channels methods. This is done in conjunction with the near–far decomposition of the resulting amplitude[1]. Such a decomposition is quite useful as it separates the repulsive, Coulomb, component of the interaction from the more useful nuclear interaction: the near–side component carrier information about the repulsive interaction (positive angles), the far–side component is

primarily sensitive to the attractive nuclear interaction (negative angles), responsible for the nuclear rainbow.

An alternative method of analysis is based on the use of a conveniently parametrized S–matrix, from which semianalytic expressions for the scattering amplitude are derived. This has been pioneered by Frahn[2] who employed this procedure primarily to the analysis of heavy ion scattering at low energies, where the near–side component plays a dominant rôle. Though Frahn has always emphasized the rôle of strong absorption and the resulting diffractive scattering in the heavy ion system, his method is general enough to accomodate strong refractive effects such as rainbows and glories. In fact Frahn and Gross[3] have layed down the grounds for a quite general and powerful framework, based directly on the S–matrix, through which nuclear refractive effects can be studied and analysed, clearly in the presence of strong absorption. Very powerful methods such as the uniform semiclassical approximation (USCA), may be easily extended to strongly absorptive media using the result of Frahn and Gross[3]. Unfortunately the F–G theory was never subjected to realistic numerical tests.

It is the purpose of this paper to supply such tests. This stems principally from the fact that only recently, the relevant intermediate energy HI elastic scattering data necessary for such tests, have become available. Further, recent data[4] and analysis[5] suggest that a further decomposition of the near and far amplitudes into retractive and diffractive components may be quite useful. As we shall show, the methods we develop in this paper enables us to perform such a decomposition in a rather simple way. In a way, our paper may also be considered as a generalization of the uniform semiclassical approximation to absorptive interactions.

Several recent theoretical work on heavy–ion elastic scattering are worth mentioning in connection with our developments. In particular, McVoy and collaborators[6] have recently done extensive work on the analysis of intermediate energy elastic scatering angular distributions through numerical study of the contribution and

interference between different physically identifiable pieces of both the near and far amplitudes. Vigezzi and Winther[7] have applied the Knoll and Schaeffer method[8] to discuss both elastic and quasielastic scattering of several heavy–ion systems. Finally, da Silveira[9] touched upon a question very close to what we discuss in the present paper, namely the modification that absorption inflicts on rainbow scattering. Our method is, however, more general.

The paper is organized as follows: In Section II, the near–far, diffraction–refraction decomposition of the scattering amplitude à la Frahn and Gross is fully reviewed. Several improvements and generalizations of the F–G formalism are also developed in this section. In Section III we introduce the powerful method of symbol calculus, necessary for practical evaluation of the refractive and diffractive components subsequently discussed and developed in Section III. In Section IV we review the uniform semiclassical approximation for the absorption free amplitude and develop asymptotic representation necessary for the application of the techniques discussed in Section III. In Section V we apply our formalism to elastic scattering of several projectiles off ^{208}Pb at intermediate energies. Finally in Section VI we present our concluding remarks.

II. THE NEAR–FAR, DIFFRACTION–REFRACTION DECOMPOSITION OF THE SCATTERING AMPLITUDE

In this section, we present in full details the formal development of the elastic scattering amplitude, up to the point where the different and diverse physical effects associated with absorption and refraction may be easily identified and considered on the same footing. Whereas Frahn emphasizes the diffractive effect of absorption for the purpose of obtaining closed expressions, other authors treat absorption approximately (semiclassically) in favor of refractive effects such as rainbow for whose treatment the uniform semiclassical approximation may be utilized.

It is our purpose in this section to present a less prejudiced discussion, within the formalism developed by Frahn and Gross. We extend further the F–G formalism in such a way as to make it amenable to a detailed numerical investigation. For this purpose and also for the extention of the uniform semiclassical approximation to the case of absorptive scattering, it is useful to find a way of relating the absorption–modified amplitude to the absorption–free one. We accomplish this below through the introduction of what may be called the diffraction operator.

We use below the notation employed by Berry[10]. The elastic scattering amplitude is

$$f(\theta) = \frac{1}{iK}\sum_{\ell=0}^{\infty}(\ell+1/2)\left[|S_\ell|\, e^{2i\delta_\ell}-1\right]P_\ell(\cos\theta) \quad . \tag{II.1}$$

Eq. (II.1) differs from the one used by Berry in an important aspect, namely that the partial wave amplitude S is allowed to have a modulus smaller than one, as unitarity requires in absorptive scattering, i.e.

$$|S_\ell| \leq 1 \quad . \tag{II.2}$$

We now proceed and decompose $f(\theta)$ into tis near and far components through the use of the following asymptotic form of the Legendre function

$$P_\ell(\cos\theta) \simeq \sqrt{\frac{2}{\pi(\ell+1/2)\sin\theta}}\ \cos\left[(\ell+1/2)\theta-\pi/4\right] \tag{II.3}$$

valid for $\ell^{-1} < \theta < \pi-\ell^{-1}$. The near–side, $f^{(+)}$, and far–side, $f^{(-)}$, components of $f(\theta)$ are just obtained from the $e^{-i(\ell+1/2)\theta}$ and $e^{i(\ell+1/2)\theta}$ branches of the cosine function in Eq. (II.3), respectively

$$f^{(\pm)}(\theta) = \frac{1}{ik\sqrt{2\pi\sin\theta}}\sum_{\lambda=1/2}^{\infty}\lambda^{1/2}\, e^{2i\delta(\lambda)}|S(\lambda)|e^{\mp i\lambda\theta}\, e^{\pm i\pi/4} \tag{II.4}$$

$$\lambda \equiv \ell+\frac{1}{2}$$

where the factor (-1) is dropped as it contributes only at $\theta=0$, a region necessarily avoided here as long as Eq. (3) for $P_\ell(\cos\theta)$ is used. The above equation can be Poisson–decomposed as

$$f^{(\pm)}(\theta) = \frac{1}{ik\sqrt{2\pi\sin\theta}}\sum_{m=-\infty}^{\infty} e^{-im\pi}\int_0^{\infty} d\lambda\, \lambda^{1/2}|S(\lambda)|$$

$$\times \exp[i(2\delta(\lambda)+2m\pi\lambda \pm \lambda\theta \pm \pi/4)] \quad . \tag{II.5}$$

For simplicity, we consider the case in which the deflection function $2(d\delta(\lambda)/d\lambda)$ never exceeds $\pm\pi$. Then the $m=0$ term in the above sum approximates very well $f^{\pm}$. Introducing the notation $\sqrt{\sin\theta}\, f^{\pm}(\theta) \equiv I^{\pm}(\theta)$, we have

$$I^{\pm}(\theta) = \frac{e^{\pm i\pi/4}}{ik\sqrt{2\pi}} \int_{-\infty}^{\infty} d\lambda\, \lambda^{1/2} |S(\lambda)| \exp[i(2\delta(\lambda) \pm \lambda\theta)] \qquad \text{(II.6)}$$

where we have extended the lower limits of the integrals to $-\infty$ (with $|S(\lambda)| = 0$ for λ=0).

It is clear from Eq. (II.6) that $I^{\pm}(\theta)$ is simply (aside from a constant) the Fourier transform of $\lambda^{1/2}|S(\lambda)|e^{2i\delta(\lambda)}$. $I^{(-)}(\theta) \equiv I^{(+)}(-\theta)$ is the Fourier transform taken as a function of $(-\theta)$ of the same λ–function. We now introduce the absorption free amplitude $I_0(\theta)$ as being the Fourier transform of $\lambda^{1/2}|S(\lambda)|e^{2i\delta(\lambda)}$

$$I_0^{\pm}(\theta) = \frac{e^{\pm i\pi/4}}{ik\sqrt{2\pi}} \int_{-\infty}^{\infty} d\lambda\, \lambda^{1/2} \exp[i(2\delta(\lambda) \mp \lambda\theta)] \quad . \qquad \text{(II.7)}$$

In order to obtain an equation which relates $I^{\pm}(\theta)$ to $I_0^{\pm}(\theta)$, we use a three–step procedure; we first inverse Fourier transform (II.6), divide over $|S(\lambda)|$ and finally Fourier transform back. Denoting the Fourier transformation of a function $G(x)$ by $F_{x\to p}G$, we have, for the near–side amplitude

$$F_{\lambda\to\theta}(|S(\lambda)|^{-1})\, F_{\theta\to\lambda}\, I_{(\theta)}^{(+)} = I_0^{(+)}(\theta) \quad . \qquad \text{(II.8)}$$

The operator $(F_{\lambda\to\theta}(|S(\lambda)|^{-1})\, F_{\theta\to\lambda})$ is an example of a class of operators called pseudo–differential[11]. As long as $|S(\lambda)|$ is representable as a polynomial in λ, the following relation holds

$$F_{\lambda\to\theta}(|S(\lambda)|^{-1})\, F_{\theta\to\lambda} = \left|S\left[i\,\frac{d}{d\theta}\right]\right|^{-1} \quad . \qquad \text{(II.9)}$$

A similar analysis follows for the far–side amplitude $I^{(-)}(\theta) \equiv I^{(+)}(-\theta)$, in which the

pseudo–differential operator is

$$F_{\lambda\to-\theta}|S(\lambda)|^{-1}\, F_{-\theta\to\lambda} = \left|S\left[i\,\frac{d}{d(-\theta)}\right]\right|^{-1} \quad . \qquad \text{(II.10)}$$

We thus find the follwoing important relation (In what follows, we drop the I superscript since $I^{(-)}(\theta) = I^{(+)}(-\theta)$.)

$$\left|S\left[i\,\frac{d}{d\theta}\right]\right|^{-1} I(\theta) = I_0(\theta) \qquad \text{(II.11)}$$

which formally solves to

$$I(\theta) = \left|S\left[i\,\frac{d}{d\theta}\right]\right| I_0(\theta) \quad . \qquad \text{(II.12)}$$

In fact, each term in the Poisson sum, Eq. (II.5) can be considered as a Fourier transform in the sense that $I^{(\pm)}(\theta) = \sum_{m=-\infty}^{\infty} e^{-i\pi m} I^{(\pm)}(\theta \mp 2m\pi) =$ $= \frac{e^{\pm i\pi/4}}{ik\sqrt{2\pi}} \int d\lambda\, \lambda^{1/2}|S(\lambda)|e^{2i\delta(\lambda)} \times e^{\mp i\lambda(\theta\mp 2\pi m)}$. Thus $\left|S\left[\pm\,\frac{id}{d\theta}\right]\right|^{-1} I^{(\pm)}(\theta \mp 2m\pi) =$ $= I_0^{(\pm)}(\theta \mp 2m\pi)$ and accordingly a relation similar to Eq. (11) is valid for the full amplitude, Eq. (II.5). It is interesting to observe that with a Fermi–shape $|S(i(d/d\theta))|$, Eq. (11) takes the appealingly simple form $e^{\Lambda/\Delta} I(\theta - i/\Delta) + I(\theta) = I_0(\theta)$, which can be solved for $I(\theta)$ as $I(\theta) = \sum_{n=1}^{\infty} I_0(\theta + (ni/\Delta))e^{-n\Lambda/\Delta}(-)^n$. We have opted for the integral equation approach to avoid dealing with complex angles.

Eq. (II.12) shows how diffraction comes into the picture as a result of the application of $|S(i(d/d\theta))|$ on the otherwise purely refractive amplitude $I_0(\theta)$. It seems natural, therefore, that an appropriate name to be given to our pseudo–differential operator, $|S(i(d/d\theta))|$, is the "diffraction operator" $\hat{D}$. For convenience, we introduce the notation

$$I(\theta) \equiv \langle\theta|I\rangle$$
$$I_0(\theta) \equiv \langle\theta|I_0\rangle \quad . \tag{II.13}$$

Thus

$$|I\rangle = \hat{D}|I_0\rangle = \int d\theta' \hat{D}|\theta'\rangle\langle\theta'|I_0\rangle \tag{II.14}$$

and

$$\langle\theta|I\rangle = \int d\theta' \langle\theta|\hat{D}|\theta'\rangle\langle\theta'|I_0\rangle \quad . \tag{II.15}$$

The matrix element $\langle\theta|\hat{D}|\theta'\rangle$ is just the Green function corresponding to Eq. (II.11). It is the degree of non–locality in $\theta-\theta'$ that determines now diffractive the scattering is. In fact, as we show below, most of the diffractive effects in $I^{\pm}(\theta)$ are contained in the principal part of the θ' integral.

We present now an analysis of the angle Green function $\langle\theta|\hat{D}|\theta'\rangle \equiv G(\theta-\theta')$. Owing to the unitarity limit of $|S(\lambda)|$, namely $|S(\lambda)| = 1$ for $\lambda > \lambda_R$, where λ_R characterizes the extent of the scatterer, it is safer to express $G(\theta-\theta')$ as a Fourier transform of $(d/d\lambda)|S(\lambda)|$. This involves explicitly extracting a pole term, $(\theta'-\theta+i\varepsilon)^{-1}$ with the small imaginary part used to guarantee convergence.

We obtain (this relation was originally obtained by Frahn and Gross[3] in a slightly different manner)

$$G(\theta-\theta') = \frac{i}{2\pi} \frac{1}{\theta'-\theta+i\varepsilon} F_{\lambda\to(\theta-\theta')}\left[\frac{d}{d\lambda}|S(\lambda)|\right] \quad . \tag{II.16}$$

The Fourier transform $F_{\lambda\to(\theta-\theta')}((d/d\lambda)|S(\lambda)|)$ measures the contribution of the surface. Sharp surfaces are characterized by δ–like behaviour of $(d/d\lambda)|S(\lambda)|$, resulting in a constant behaviour of $F_{\lambda\to(\theta-\theta')}\, d/d\lambda|S(\lambda)|$. Diffused surfaces give rise to a wider distribution in $\theta'-\theta$. For the purpose of illustration, we take $|S(\lambda)|$ to be a Fermi

function $|S(\lambda)| = [\exp[\lambda_R-\lambda]/\Delta + 1]^{-1}$. Δ here measures the extent of the surface region in angular momentum space. Semiclassically, it is approximately given by ka with a being the diffuseness of the density profile of the scatterer and k the asymptotic wave number. We find[12,13]

$$F_{\lambda\to(\theta-\theta')}\left[\frac{d}{d\lambda}|S(\lambda)|\right] = \frac{\pi\Delta(\theta'-\theta)}{\sinh[\pi\Delta(\theta'-\theta]} \exp[i\lambda_R(\theta'-\theta)]$$
$$= A(\Delta(\theta'-\theta)) \exp[i\lambda_R(\theta'-\theta)] \quad , \tag{II.17}$$

where we have introduced the damping function

$$A(x) = \frac{\pi x}{\sinh \pi x} \quad . \tag{II.17'}$$

Thus, very diffused systems ($\Delta \gg 1$) are characterized by a small non–locality in $G(\theta-\theta')$, since one has

$$G(\theta-\theta') \simeq \frac{i}{\pi} \lim_{\varepsilon\to 0} \frac{1}{\theta'-\theta+i\varepsilon} \pi\Delta(\theta-\theta')\, e^{-\pi\Delta|\theta-\theta'|} \times e^{i\lambda_R(\theta'-\theta)} \quad , \tag{II.18}$$

even for θ' very close to θ. The degree of non–locality in θ, and accordingly the degree of diffraction, is measured by $(1/\pi\Delta)$. The above situation represents a case of weak diffraction (the largeness of Δ forces G to be dominated by its on–shell part).

The other extreme $\Delta \to 0$, gives

$$G(\theta-\theta') \xrightarrow{\Delta\to 0} \frac{i}{2\pi} \lim_{\varepsilon\to 0} \frac{1}{\theta'-\theta+i\varepsilon} e^{i\lambda_R(\theta'-\theta)} \quad , \tag{II.19}$$

namely "infinite" non–locality. This would represent an extreme case of diffractive scattering such as the case in Fraunhoffer diffraction.

From the above discussion, it would seem natural to extract what we may call the diffractive component of the scattering amplitude, from the contribution to the amplitude arising from the off–shell part of the angle propagator. Writing the Green function $G(\theta-\theta')$

$$G(\theta-\theta') = G_{on}(\theta-\theta') + G_{off}(\theta-\theta')$$

$$G_{on}(\theta-\theta') = \tfrac{1}{2}\,\delta(\theta'-\theta)\,\mathcal{F}_{\lambda\to(\theta'-\theta)}\left[\frac{d}{d\lambda}\,|S(\lambda)|\right]$$

$$G_{off}(\theta-\theta') = \frac{i}{2\pi}\,P\,\frac{1}{\theta-\theta'}\,\mathcal{F}_{\lambda\to(\theta'-\theta)}\left[\frac{d}{d\lambda}\,|S(\lambda)|\right] \qquad \text{(II.20)}$$

where <u>on</u> and <u>off</u> refer to the on–shell (delta function) and off–shell (principal integral) parts, respectively, we define the diffractive component, $I_D(\theta)$ of $I(\theta)$ as the stationary phase contribution to $I_{off}(\theta)$ (where I_{off} is I calculated with G replaced by G_{off}, Eq. (II.20). Thus

$$I_D(\theta) \simeq \frac{i}{2\pi}\,\frac{A(\Delta(\theta_\Lambda-\theta))}{\theta_\Lambda-\theta}\int d\theta'\, e^{i\lambda_R(\theta'-\theta)}\, I_0(\theta') \quad . \qquad \text{(II.21)}$$

Accordingly, the refractive component, I_R of $I(\theta)$ is a sum of the on–shell piece of I and the remainder of its principal part

$$I_R(\theta) = \tfrac{1}{2}\,I_0(\theta) + \frac{i}{2\pi}\int d\theta'\left[\frac{A(\Delta(\theta'-\theta))}{\theta'-\theta} - \frac{A(\Delta(\theta_\Lambda-\theta))}{\theta_\Lambda-\theta}\right] e^{i\Lambda(\theta'-\theta)}\, I_0(\theta') \quad . \qquad \text{(II.22)}$$

Equations (II.21) and (II.22) are valid for angles larger than θ_Λ, which is the

stationary point angle obtained from the condition

$$\frac{d}{d\theta'}\,[\Lambda\theta' + \text{phase of } I_0(\theta')]_{\theta'=\theta_\Lambda} = 0 \quad . \qquad \text{(II.23)}$$

If $I_0(\theta')$ is dominated by a stationary phase then θ_Λ is just the corresponding classical deflection function. However, Eq. (21) can be used in a more general sense. For instance if there are more than one s.p., I_D becomes a sum of their contributions. We remind the reader that our refractive component I_R is ***not*** the absorption free amplitude $I_0(\theta)$, since it is modified by absorption through the second term in Eq. (II.22).

Whereas Eq. (II.21) for $I_D(\theta)$ is readily calculable once $I_0(\theta)$ is known, not so for $I_R(\theta)$, Eq. (II.22). The principal part integral is cumbersome to evaluate numerically. For this purpose we develop in the next section an alternative and apparently more poweful techniques which will enable us to evaluate refractive component of the scattering amplitude. This technique is known as symbol calculus and it has been recently reviewed by McDonald[14].

III. PHASE SPACE EQUATION, SYMBOLS AND THE REFRACTIVE AMPLITUDE

In the preceding section we presented a general method for the separation of the near– or far–side amplitudes into a diffractive and a refractive components. The form obtained for the refractive component is not very convenient from the numerical point of view (of course one may obtain it by merely subtracting $I_p(\theta)$ from the total amplitude. However our aim is to develop a full theory of these components).

In the present section our goal is to develop a scheme through which the refractive component can be calculated easily, given the general structure of the absorption–free amplitude. To achieve this goal, our strategy will be to go back to our pseudo–differential equation, to construct eikonal (WKB) approximate solution for it, resorting to phase space and symbol techniques. The method to do this is described in a recent *Physics Reports* by S.W. McDonald[14].

The first thing we have to do is to derive an equation which envolves only operators. Our basic equation, (II.11), is an equation for the vector $|I\rangle$, but if we multiply it by its conjugate we readily obtain the equation

$$D^{-1}|I\rangle\langle I| = |I_0\rangle\langle I_0|D^{+} \tag{III.1}$$

for the operator $|I\rangle\langle I|$, where D^{-1} and D^{+} are the inverse and the adjoint of the diffraction operator. We observe that the diagonal elements of the projectors $|I\rangle\langle I|$ and $|I_0\rangle\langle I_0|$ are just the complete and absorption–free cross sections.

The rule to construct a symbol of an operator may be derived from the relation between the diffraction operator and its symbol. It is easily found that if $Q(\theta,\theta')$ is an operator and $q(\theta,\lambda)$ its symbol we have

$$q(\theta,\lambda) = \int_{-\infty}^{\infty} ds\, Q(\theta,\theta-s)\, e^{i\lambda s} \tag{III.2}$$

and, inversely

$$Q(\theta,\theta') = \int \frac{d\lambda}{2\pi} q(\theta,\lambda)\, e^{-i\lambda(\theta-\theta')} \tag{III.3}$$

In fact, it is readily verified that in the case of $\hat{D}$ which has the explicit representation

$$D(\theta,\theta') = \int_{-\infty}^{\infty} \frac{d\lambda}{2\pi} |S(\lambda)|\, e^{-i\lambda(\theta-\theta')} \tag{III.4}$$

we obtain from Eq. (III.2) the symbol

$$d(\theta,\lambda) = \int_{-\infty}^{\infty} ds \int_{-\infty}^{\infty} \frac{d\lambda'}{2\pi} |S(\lambda')|\, e^{-i(\lambda'-\lambda)s} = |S(\lambda)| \tag{III.5}$$

as it should.

For the projectors $|I\rangle\langle I|$ and $|I_0\rangle\langle I_0|$, Eq. (III.2), gives respectively the symbols

$$s(\theta,\lambda) = \int_{-\infty}^{\infty} ds\, I(\theta)\, I^{*}(\theta-s)\, e^{i\lambda s} = 2\pi\, I(\theta)\, \tilde{I}^{*}(\lambda)\, e^{i\lambda\theta} \tag{III.6}$$

and

$$s_0(\theta,\lambda) = 2\pi\, I_0(\theta)\, \tilde{I}_0^{*}(\lambda)\, e^{i\lambda\theta} \quad . \tag{III.7}$$

We obtain now the rule to construct the symbol of the adjoint of an operator. By definition,

$$q^+(\theta,\lambda) = \int ds\, Q^+(\theta,\theta-s)\, e^{i\lambda s} \tag{III.8}$$

with

$$Q^+(\theta,\theta') = Q^*(\theta',\theta) \quad . \tag{III.9}$$

Using Eq. (III.3) we get

$$q^+(\theta,\lambda) = \int_{-\infty}^{\infty} ds\, \frac{d\lambda'}{2\pi}\, q^*(\theta-s,\lambda')\, e^{-i(\lambda'-\lambda)s} \quad . \tag{III.10}$$

Expanding $q^*(\theta-s,\lambda')$ about θ in its first variable, we derive after some manipulations, the result

$$q^+(\theta,\lambda) = e^{i\vec{\partial}_\lambda \vec{\partial}_\theta}\, q^*(\theta,\lambda) \tag{III.11}$$

where $\vec{\partial}_\lambda$ and $\vec{\partial}_\theta$ stand for the derivatives of the function at the right and the exponential operator is defined by its Taylor series. Since the diffraction operator is real and its symbol is independent of θ, the formula above gives

$$d^+(\theta,\lambda) = |S(\lambda)| \quad . \tag{III.12}$$

Obviously, the symbol of the inverse operator is just the inverse of the symbol of the operator. Thus we have defined the symbols of the operators which enter in Eq. (III.1). However we still need the rule to construct the symbol of a product from the symbols of the factors. We proceed now to derive it.

Let $Q_1(\theta,\theta')$ and $Q_2(\theta,\theta')$ be two operators, $q_1(\theta,\lambda)$ and $q_2(\theta,\lambda)$ their symbols, and $q(\theta,\lambda)$ the symbol of their product, then, since

$$(Q_1Q_2)(\theta,\theta') = \int d\theta''\, Q_1(\theta,\theta'')\, Q_2(\theta'',\theta') \tag{III.13}$$

we have

$$q(\theta,\lambda) = \int ds\, d\theta''\, Q_1(\theta,\theta'')\, Q_2(\theta'',\theta-s)\, e^{i\lambda s} \quad . \tag{III.14}$$

Expressing Q_1 and Q_2, using Eq. (III.3), in terms of their symbols we get after integrating in ds

$$q(\theta,\lambda) = \int d\theta''\, \frac{d\lambda'}{2\pi}\, q_1(\theta,\lambda)\, q_2(\theta'',\lambda)\, e^{-i(\lambda'-\lambda)(\theta-\theta'')} \quad . \tag{III.15}$$

Making the substitutions $\theta'' = \theta+s$ and $\lambda' = \lambda+q$ we find

$$q(\theta,\lambda) = \int ds\, \frac{dq}{2\pi}\, q_1(\theta,\lambda+q)\, q_2(\theta+s,\lambda)\, e^{iqs} \quad . \tag{III.16}$$

Expanding q_1 about λ in its second variable and q_2 about θ in its first variable we deduce after standard calculations, the relation

$$q(\theta,\lambda) = q_1(\theta,\lambda)\, e^{\overleftarrow{i\partial}_\lambda \vec{\partial}_\theta}\, q_2(\theta,\lambda) \tag{III.17}$$

where the exponential operator is defined, as before, by its Taylor series and the arrows indicate to which function the derivatives are to be applied.

Using the results we have just derived we find

$$|S(\lambda)|^{-1}\, e^{\overleftarrow{i\partial}_\lambda \vec{\partial}_\theta}\, I(\theta)\, \tilde{I}^*(\lambda)\, e^{i\lambda\theta} = I_0(\theta)\, \tilde{I}_0^*(\lambda)\, e^{i\lambda\theta}\, e^{\overleftarrow{i\partial}_\lambda \vec{\partial}_\theta}\, |S(\lambda)| \tag{III.18}$$

Since $|S(\lambda)|$ does not depend on θ, the right hand side simplifies and we can also drop the common factor $\tilde{I}^*(\lambda)$ in both sides of the equation, which is written finally as

$$|S(\lambda)|^{-1} e^{i\overleftarrow{\partial}_\lambda \overrightarrow{\partial}_\theta} I(\theta)\, e^{i\lambda\theta} = I_0(\theta)\, e^{i\lambda\theta} \quad . \tag{III.19}$$

This is the phase space representation of the Eq. (III.1).

This phase–space equation may be understood as a linear inhomogeneous differential equation of infinite order. It is easy to prove that its Green's function is just the same of the original pseudo–differential equation and consequently it is possible to write down its solution immediately but this will not lead us to anything new, what we intend is to use it to generate approximate asymptotic solutions. To do this, we make the assumption of the eikonal theory that the approximate solution we are looking for has the form

$$I(\theta) = C(\theta)\, e^{i\phi(\theta)} \tag{III.9}$$

where $C(\theta)$ is a slowly varying function of θ while $\phi(\theta)$ varies rapidly in the semiclassical regime. Substituting then this ansatz into the equation and collecting terms of the same order in both sides of it we determine $C(\theta)$ and $\phi(\theta)$.

Before substituting $I(\theta)$, we observe that the diffraction term we defined in the preceding section is a homogeneous solution of Eq. (III.19) for $\theta \neq \theta_\Lambda$. Of course, this follow from the fact that it is just the Green's function of Eq. (II.11). It is then possible to interpret the diffraction contribution as the solution of Eq. (III.19) with no source. Inserting Eq. (III.9) into Eq. (III.19) with the r.h.s. zero we obtain

$$\sum_{n=0}^{\infty} \frac{i^n}{n!} \frac{d^n |S(\lambda)|^{-1}}{d\lambda^n} \frac{\partial^n}{\partial\theta^n} \left\{ C(\theta)\, e^{i[\phi(\theta)+\lambda\theta]} \right\} = 0 \quad . \tag{III.20}$$

The leading order series in the equation above come from the derivatives of the exponential and their sum is just a Taylor series expansion which gives the result

$$\left| S\left[-\frac{d\phi}{d\theta} \right] \right|^{-1} = 0 \quad . \tag{III.21}$$

This means that the diffractive contribution comes from the angular momenta which are the poles of the S–matrix. Let us now consider the source term in the r.h.s. of Eq. (III.19). First we suppose that the purely reffractive amplitude, $I_0(\theta)$, is already calculated asymptotically in such way, that it can be written as a sum of eikonal terms, that is, as

$$I_0(\theta) = \sum_i C_i(\theta)\, e^{i\phi_i(\theta)} \tag{III.22}$$

where each term comes from a stationary phase contribution to the amplitude or, physically, from a semiclassical trajectory (in the next section, we discuss how this can be done in the case of rainbow scattering). Inserting this expression for $I_0(\theta)$ into Eq. (III.19) we find that a solution can be constructed if we impose that to each term of $I_0(\theta)$ corresponds an equivalent term of the total amplitude $I(\theta)$ with the same phase but with a magnitude $A_i(\theta)$ which is given by

$$I_R(\theta) = \sum_i A_i(\theta) = \sum_i \left| S\left[-\frac{d\phi_i}{d\theta} \right] \right| C_i(\theta)\, e^{i\phi_i(\theta)} \quad . \tag{III.23}$$

As we shall show in the next section, even in the case of a caustic (rainbow scattering), which requires the use of the uniform semiclassical approximation, the amplitude $I_0(\theta)$ may be represented as (III.22), with slowly varying factors $C_i(\theta)$. In

the dark–side of the rainbow, however, care must be taken when applying (III.23) to construct $I_R(\theta)$.

Summarizing this section we have found that asymptotically the total elastic amplitude may be expressed as a sum of the diffractive term, derived in the preceding section, plus the refractive components which are just the contribution of the semiclassical trajectories of the absorption–free scattering damped by the absorption.

IV. EIKONAL REPRESENTATION OF THE UNIFORM SEMICLASSICAL ABSORPTION–FREE AMPLITUDE

As already has been announced in the previous section, it is important for the construction of $I_R(\theta)$, Eq. (III.23), that the absorption–free amplitude is represented in an eikonal form namely as a sum of terms involving a slowly varying amplitude multiplying a more rapidly varying phases, Eq. (III.22).

The purpose of this section is to supply the necessary background for constructing the eikonal representation of $I_0(\theta)$. This background involves both the stationary phase method in its simplest form, as well as the uniform asymptotic representation necessary for the treatment of caustics (rainbows).

In the case of a monotonically varying deflection function (generally defined as $2\frac{d\delta_\lambda}{d\lambda}$ where δ_λ is the phase shift), the contribution to $I_0(\theta)$ mainly comes from an stationary phase point, λ_i, which is a solution of the equation

$$\Theta(\lambda_i) \equiv 2\frac{d\delta_\lambda}{d\lambda}\bigg|_{\lambda=\lambda_i} = \theta \tag{IV.1}$$

and, physically, corresponds to the angular momentum of a semiclassical trajectory. Following Erderlyi's[15] presentation of the stationary phase method we map the phase shift onto a quadratic function, that is,

$$2\delta(\lambda) - \lambda\theta = \mp t^2 + B(\theta) \tag{IV.2}$$

where $+(-)$ if $\Theta'(\lambda_i)$ positive (negative) and

$$B(\theta) = 2\delta(\lambda_i) - \lambda_i\theta \tag{IV.3}$$

since by construction $t=0$ when $\lambda=\lambda_i$ The amplitude then becames

$$I_0(\theta) = e^{i[2\delta(\lambda_i)-\lambda_i\theta]} \int_{-\infty}^{\infty} dt\, \lambda^{1/2}(t)\, \frac{d\lambda}{dt}(t)\, e^{\mp it^2} \qquad (IV.4)$$

where we have extended the lower limit of integration to infinity using the fact that owing to the rapid oscillations of the integrand, only a small region around $t=0$ contributes to the integral. Substituting the coefficient $\lambda^{1/2}(t)\,\frac{d\lambda}{dt}(t)$ by the first term of its expansion about $t=0$, i.e.,

$$\lambda^{1/2}(0)\,\frac{d\lambda}{dt}(0) = \sqrt{\frac{2\lambda_i}{\mp\theta(\lambda_i)}} \qquad (IV.5)$$

calculated taking the second derivative of the equation defining the mapping, we can perform the integration in dt to obtain

$$I_0(\theta) \simeq \sqrt{\frac{2\pi\lambda_i}{-\theta(\lambda_i)}}\; e^{i[2\delta(\lambda_i) - \lambda_i\theta \mp \frac{\pi}{4}]} \qquad (IV.6)$$

which is the usual single stationary phase approximation.

According to the recipe of the preceding section, in the total amplitude, this term will appear damped by the factor $|S(\lambda_i)|$, Eq. (III.23), with λ_i replaced by $\lambda_i(\theta)$, since $\frac{d\phi(\theta)}{d\theta}$ in this case is just

$$\frac{d}{d\theta}\left\{2\delta[\lambda_i(\theta) - \lambda_i(\theta)\theta\right\} = \lambda_i(\theta) \quad . \qquad (IV.7)$$

To derive the eikonal representation of rainbow scattering, we review first the uniform semiclassical approximation deduced by Berry[10], adapting to the scattering

formalism, a mathematical formula obtained by Chester, Friedman and Ursell[16]. The uniform semiclassical approximation is, in fact, a generalization for the case of two stationary points of Erderlyi's method. The mapping of the phase–shift is now made onto a cubic function, namely,

$$2\delta(\lambda) - \lambda\theta = \frac{\mu^3}{3} + x(\theta)\mu + A(\theta) \qquad (IV.8)$$

where $x(\theta)$ and $A(\theta)$ are determined from the values of the phase at the stationary points. Taking the derivative of Eq. (IV.8) we have

$$\frac{d\lambda}{d\mu}\,[\theta(\lambda)-\theta] = \mu^2 + x(\theta) \qquad (IV.9)$$

where the l.h.s. vanishes at the two angular momenta which we denote by λ_1 and λ_2 and the r.h.s. at $\mu = \pm\sqrt{-x}$. The quantity $x(\theta)$ may be fixed such that it is negative when the λ's are real, that is, in the so called illuminated zone of the rainbow and, positive in the dark zone, where the two stationary values are complex conjugates. Associating λ_1 with the root $\sqrt{-x}$ and λ_2 with $-\sqrt{-x}$ we deduce, easily, the expressions

$$A(\theta) = \frac{2\delta[\lambda_1(\theta)] - \lambda_1(\theta)\theta + 2\delta[\lambda_1(\theta) - \lambda_1(\theta)\theta}{2} \qquad (IV.10)$$

and

$$x(\theta) = -\left\{\frac{3}{4}\,[2\delta(\lambda_2) - \lambda_2\theta - 2\delta(\lambda_1) + \lambda_1\theta]\right\}^{2/3} \qquad (IV.11)$$

for the illuminated zone, and in the dark zone these equations may be prolonged with the association of λ_1 to $i\sqrt{x}$ and λ_2 to $-i\sqrt{x}$, which leaves Eq. (IV.10), for $A(\theta)$, unchanged and for $x(\theta)$ gives

$$x(\theta) = \left\{ \frac{3}{4} \left[2\delta(\lambda_1) - \lambda_1\theta - 2\delta(\lambda_2) + \lambda_2\theta \right] \right\}^{2/3} . \qquad \text{(IV.12)}$$

At this point, we have to say how to choose the two λ's. We note that in the near–side the μ–axis is reverse to the λ–axis: the $+\infty$ of the λ corresponding to the $-\infty$ of μ. This implies that to be consistent we must have $\lambda_1 < \lambda_2$ in the bright region and $\mathrm{Im}\,\lambda_1 < 0$, in the shadow region, for the near–side amplitude. On the other hand, for the far–side, we take the λ's such that $\lambda_2 > \lambda_1$ and $\mathrm{Im}\,\lambda_1 > 0$, for the illuminated and the shadow regions, respectively.

Substituting, then, μ for λ, using the equation defining the mapping, the near and the far–side amplitudes that we denote by the superscript (+) and (−), respectively, are given by

$$I_r^{(\pm)}(\theta) = (\mp)\, e^{iA(\theta)} \int_{-\infty}^{\infty} d\mu\, \lambda^{1/2}(\mu) \frac{d\lambda}{d\mu}(\mu)\, e^{i\left(\frac{\mu^3}{3} + x\mu\right)} \qquad \text{(IV.13)}$$

where the subscript r referes to rainbow scattering and the only approximation is the extension of the limits of integration from $-\infty$ to $+\infty$, which is justified, again, by the assumption that the contribution to the integral come from the vicinities of the stationary phase values. The next step is to substitute the function $\lambda^{1/2}(\mu) \frac{d\lambda}{d\mu}(\mu)$ by its Taylor series

$$\lambda^{1/2}(\mu) \frac{d\lambda}{d\mu}(\mu) = \sum_{m=0}^{\infty} (\mu^2 + x)^m (p_m + q_m \mu) \qquad \text{(IV.14)}$$

about the two roots $\pm\sqrt{-x}$ retaining only the first term, m=0. The coefficients p_0 and q_0 are easily determined, taking the second derivative of Eq. (IV.9), to be given by

$$p_0 = \mp \frac{1}{2} \left[\sqrt{\frac{2\lambda_1\mu_0}{\theta''(\lambda_1)}} + \sqrt{\frac{2\lambda_2\mu_0}{-\theta''(\lambda_2)}} \right] \qquad \text{(IV.15)}$$

and

$$q_0 = \mp \frac{1}{2\mu_0} \left[\sqrt{\frac{2\lambda_1\mu_0}{\theta''(\lambda_1)}} + \sqrt{\frac{2\lambda_2\mu_0}{-\theta''(\lambda_2)}} \right] \qquad \text{(IV.16)}$$

where $\mu_0 = \sqrt{-x}$ in the illuminated region, and in the shadow region $\mu_0 = i\sqrt{x}$. With these substitutions we arrive at the final asymptotic expressions for the amplitudes

$$I_r^{(\pm)}(\theta) = (\pm)\, 2\pi\, e^{iA(\pm\theta)} \left\{ p_0\, \mathrm{Ai}[x(\pm\theta) - i\, q_0\, \mathrm{Ai}'[x(\pm\theta)] \right\} \qquad \text{(IV.17)}$$

where Ai(x) and Ai'(x) are the Bessel function of fractional order and its derivative, usually known as the Airy function, defined by

$$\mathrm{Ai}(x) = \frac{1}{2\pi} \int_0^{\infty} d\mu \cos\left[\frac{\mu^3}{3} + x\mu \right] . \qquad \text{(IV.18)}$$

The formula above describes the passage from the region "illuminated" by the two trajectories where the cross section presents typical oscillations caused by their interference to the dark–side of the rainbow penetrated only by a exponentially decaying trajectory. It is easy to show using the asymptotic expression of the Airy function, valid for large negative expression of values of its argument that away from the rainbow, in the "bright–side", the amplitudes reduce to a sum of two terms given by Eq. (IV.6). In the dark–side, on the other hand, far from the rainbow angle, substitution of the Airy function by its asymptotic expression for large positive argument, show that the amplitudes decay exponentially as

$$I^{(\pm)}(\theta) \sim e^{-[\theta \mathrm{Im}\lambda_1]} . \qquad \text{(IV.19)}$$

Let us cast the uniform semiclassical approximation for the rainbow scattering in the form of a sum of eikonal terms, i.e., a phase factor times a coefficient. To do this we use the formula of Abramovitch and Stegun[17] which express the Airy function and its derivative asyntotically as

$$\mathrm{Ai}(x) = f_1 \cos u + f_2 \sin u \tag{IV.20}$$

and

$$\mathrm{Ai}'(x) = g_1 \sin u - g_2 \cos u \tag{IV.21}$$

for $x < 0$, where $u = 2(-x)^{3/2}/3$, while for $x > 0$

$$\mathrm{Ai}(x) = f \exp(-2x^{3/2}/3) \tag{IV.22}$$

and

$$\mathrm{Ai}'(x) = -g \exp(-2x^{3/2}/3) \quad . \tag{IV.23}$$

The first two equations, (IV.20) and (IV.21), are inverted introducing the Airy function $\mathrm{Bi}(x)$ and its derivative $\mathrm{Bi}'(x)$, which gives

$$f_1 = \mathrm{Ai} \cos u - \mathrm{Bi} \sin u \quad , \tag{IV.24}$$

$$f_2 = \mathrm{Ai} \sin u + \mathrm{Bi} \cos u \quad , \tag{IV.25}$$

$$g_1 = \mathrm{Ai}' \sin u + \mathrm{Bi}' \cos u \quad , \tag{IV.26}$$

and

$$g_2 = -\mathrm{Ai}' \cos u + \mathrm{Bi} \sin u \quad . \tag{IV.27}$$

In fig. 1 we show all these functions together with the phases. We see that, apart from a small region around $x=0$, they indeed vary slowly as compared to the phases.

Writing the two trigonometric functions in terms of exponentials we will have the eikonal form for the uniform semiclassical approximation. To apply then the recipe of the preceding section we need, for $x < 0$,

$$\frac{d}{d\theta}(A \pm \mu) = \frac{dA}{d\theta} \pm \frac{dx}{d\theta}\frac{d\mu}{dx} \tag{IV.28}$$

where $\frac{dA}{d\theta} = (\lambda_1+\lambda_2)/2$ and $\frac{dx}{d\theta} = (\lambda_1+\lambda_2)/2\sqrt{-x}$, which yields

$$\frac{dA}{d\theta} = \lambda_1 \quad \text{for} \quad (+) \quad \text{and} \quad \frac{dA}{d\theta} = \lambda_2 \quad \text{for} \quad (-) \quad . \tag{IV.29}$$

In the shadow, $x > 0$,

$$\frac{dA}{d\theta} = \frac{\lambda_1+\lambda_2}{2} + i\sqrt{x}\frac{dx}{d\theta} = \lambda_1 \quad . \tag{IV.30}$$

Reexpressing then the exponentials as trigonometric function we obtain the modified uniform expression for the refractive rainbow scattering

$$I_R^{\pm}(\theta) = \mp \exp(iA)\Big[p_0(|S(\lambda_1)|+|S(\lambda_2)|)\mathrm{Ai} - i(|S(\lambda_1)|-|S(\lambda_2)|)\mathrm{Bi}\Big] +$$

$$- i\, q_0\Big[(|S(\lambda_1)|+|S(\lambda_2)|\mathrm{Ai}' - i(|S(\lambda_1)|-|S(\lambda_2)|)\mathrm{Bi}'\Big] \tag{IV.31}$$

in the illuminated side of the rainbow and

$$I_R^{\pm}(\theta) = \mp|S(\lambda_1)| \exp(iA)(p_0\,\mathrm{Ai} - i\,q_0\,\mathrm{Ai}') \tag{IV.32}$$

in the shadow.

Before we apply our theory to data analysis (done in the next section) we first check the validity of our semiclassical formalism by applying it to a typical heavy–ion case. Let us take as an example the McIntyre parametrization of the S–matrix element, given by

Mermaz for the system $^{16}O+^{40}Ca$[18] (see Table I). Just for illustrative purposes we increase the nuclear rainbow making the parameter $\mu = 10$ (actually we discuss the real case in the next section) in order to see the first minimum of the rainbow. The deflection and the profile functions are shown in fig. 6. The comparison with the exact partial wave sum is in fig. 2, where the absorption free cross section is also exhibited. The semiclassical amplitude contains the diffractive term plus the contributions of the two rainbows and of the internal trajectory. In fig. 3 we show the near and the far components, approximated and exact and, in the two following figures 4 and 5 we decompose them in their refractive and diffractive sub–components. We can see that the damping caused by the absorption destroys the oscillation in the nuclear rainbow. We conclude from these figures that our formalism describes very well the fall–off in the shadow of the rainbows. In the vicinity of $\theta = \theta_\Lambda$ we are ovbiously overestimating the diffractive contribution.

V. APPLICATIONS

We apply now the results we have obtained in the preceding sections to analyse a set of elastic angular distributions pertaining to four different systems at intermediate energies. In the first two systems the ^{16}O at the laboratory energy of 1503 MeV is the projectile and the targets are ^{40}Ca and ^{90}Zr and, in the two others cases, ^{12}C at 2400 MeV is the projectile and ^{12}C and ^{208}Pb are the targets. The data points for these systems were fitted in references 18 and 19, respectively, using a McIntyre parametrization of the S–matrix, i.e., the nuclear S–matrix was taken to be of the form

$$S_\ell^N = \left[\exp\left[\frac{\Lambda-\ell}{\Delta}\right] + 1\right]^{-1} \exp\left\{2d_1\left[\exp\left[\frac{\ell-\Lambda_1}{\Delta_1}\right] + 1\right]^{-1}\right\}$$

where the values of the parameters Λ, Δ, d_1, Λ_1 and Δ_1 which give the best fit to the data, for the four cases are shown in table I. In figures 7, 8 and 9 we show the fit of data points for the four systems.

One common feature of these systems is that, due to the projectiles' high energy, the cross–sections are concentrated in forward angles. We observe, as we should expect the Sommerfeld parameter has small values for the four cases but it increases as the target becomes heavier. As a consequence the electromagnetic interaction turns out to be more important, or, using Frahn's optical image, the diverging lens created by the Coulomb repulsion becomes more effective, in such a way that we go from the refractive far–side dominated system $^{16}O+^{12}C$ to the diffractive near–side dominated $^{12}C+^{208}Pb$, as our analysis will show in the sequel.

Following the usage employed by McVoy and collaborators in a series of recent articles[6], we plot the natural logarithm of the cross sections $\frac{d\sigma}{d\theta}$ (in units of mb) as a

function of the angle. without dividing them by the Rutherford cross–section as is more commonly done. This exhibits the exponential behaviour in the shadows more clearly. For each of the four cases we present the near–far decomposiiton of the total cross section and the diffraction–refraction decomposition of both, the near and the far–side cross sections. The semiclassical cross sections were calculated with the closed formalism of section IV. The total cross section evaluated performing the partial wave sum, i.e., the exact cross section appear in the figures as triangle dots. We discuss now the results obtained for each system.

V.1. $^{16}O + {}^{40}Ca$

In fig. 14 we show the profile function, i.e., the modulus of the S–matrix as a function of the angular momentum and the deflection function calculated with the parameters of the Table I. The Coulomb and the nuclear rainbow angles are respectively: $\theta_C = 1.18^o$ and $\theta_N = -4.99^o$ and, the critical angle associated with the angular momentum Λ is $\theta_\Lambda = 0.08$. In fig. 10 we see the total cross section and its near–far decomposition. The elastic cross section exhibits the characteristic Fraunhofer oscillations which are more pronounced in the region of the crossover angler, approximately 4.5°, and disappear as the scattering angle increases with the cross section becoming far–side dominated. We observe also from fig. 10 that the semiclassical calculation reproduces very well the exact partial wave sum.

In fig. 11, the decomposituon of the near–side cross section shows that the refractive subcomponent associated with the broad Coulomb rainbow is dominant at forward angles with a small interference with the diffractive subcomponent. Its fall–off is steeper than that of the diffraction. This may be understood looking at fig. 13, where we show the paths in the complex angular momentum plane of the angular momenta of the complex trajectories in the shadows of the two rainbows. We see that the imaginary part for the Coulomb rainbow goes rapidly to $-\pi\Delta_1$ which is the imaginary part of the pole of the

defelection function. Since $\Delta \gtrsim \Delta_1$ the diffraction exponential decaying should be sligthly faster than in the rainbow shadow. We observe also that for angles $\theta \gtrsim 11^o$ is the contribution of the internal trajectory which prevails. This contribution tends to be just a Rutherford damped cross section. Nevertheless, we remark that the cross section in this angle region is extremely small and beyond the measured angular spectrum, therefore, we do not know the physical content of the model in this angular domain.

In fig. 12 we present the decomposition of the far–side cross section. The diffractive subcomponent decays rapidly becoming negligible for angles $\theta \gtrsim 8^o$. We see in fig. 13 that the imaginary part of angular momentum of the complex trajectory in the shadow of the nuclear rainbow is smaller than $\pi\Delta/3$ for $\theta < 8^o$. The period of the diffraction–refraction interference in forward angles is $180^o/(\Lambda - \Lambda_I) \simeq 4^o$.

V.2. $^{16}O + {}^{90}Zr$

The characteristic of the angular distribution of this system as can be seen in fig. 15, is the presence of Fraunhoffer oscillations which extend over the entire angular spectrum. Of course, this is a consequence of the fact that the near– and the far–side components are comparable over a large angular domain as can be seen in the figure. The deflection function, in fig. 19, shows that the two rainbows are very symmetric: the rainbow angles are $\theta_C = 1.77^o$ and $\theta_N = 1.52^o$. The Coulomb rainbow is broader but the narrow nuclear rainbow is in the diffraction shadow with $\theta_\Lambda = 0.2^o$.

We see in fig. 16 that the near–side is diffractive at small angles, $\theta \lesssim 7$, and refractive for $\theta \gtrsim 7$. The fall–off in the shadow of Coulomb rainbow is steeper than that of the diffraction. In fig. 18, we see that this is explained by the fact that the pole of $|S(\lambda)|$ is inside the curve described by the angular momentum of the complex trajectory.

The situation of the far–side component, see fig. 17, is opposite of the near–side: it is diffractive at forward angles and become refractive as the scattering angle increases. The interference of the two subcomponent produces a minimuim around $\theta \sim 6.5^o$.

V.3. $^{12}C + ^{12}C$. $E_{lab} = 2400$ MeV

We start now the analysis of the two systems which have the ^{12}C at the laboratory energy of 2400 MeV as projectile. We see in fig. 20 that when the target is ^{12}C the angular distribution at this high energy is far–side dominated presenting the typical Fraunhoffer oscillations which are damped as the scattering angle increases. The deflection function, in fig. 23, shows how concentrated at forward angles the system is: the two rainbow angles are, respectively, the Coulomb and the nuclear, $\theta_C = 0.28^o$ and $\theta_N = -0.56^o$. We observe also from this figure that the nuclear rainbow is partially in the illuminated side of absorption.

In fig. 21 we see the interplay of the three subcomponents that constitute the near–side cross section. The refractive contribution associated with the Coulomb rainbow is dominant at extreme forward angles, $\theta \lesssim 2^o$, but its fall–off is steeper than that of the diffractive term. Again this is explained by the fact that $\Delta < \Delta_I$, see Table I. As the angle increases the contribution of the internal trajectory becomes more important and is dominant for $\theta \lesssim 11^o$. At these relatively large angles the near–side cross section presents oscillations caused by the interference of three subcomponents.

In fig. 22, we can see how the diffractive and the refractive contributions form the far–side cross section. We verify that apart from small angles where our method overestimates the diffractive contribution the subcomponent associated with the nuclear rainbow dominates.

V.4. $^{12}C + ^{208}Pb$, $E_{lab} = 2400$ MeV

The first observation we make about fig. 24 is that, apart from the small region around the critical angle $\theta_\Lambda = 1.5^o$, our semiclassical calculation nicely reproduces the exact partial wave sum. The total cross section is near–side dominated as we preview in the introduction of this section. For angle $\theta < \theta_\Lambda$ we see, in fig. 25, that the near–side is refractive, actually, this cross section is just the Rutherford cross section. In the dark side

of the diffraction, i.e., $\theta > \theta_\Lambda$, the diffractive subcomponent is only slightly greater than the contribution from the Coulomb rainbow and both contribute to the total cross section. For larger angles, the internal trajectory is also present and for $\theta > 5^o$ it dominates. It is interesting to remark that this system has a typical Fresnel pattern but with the difference that we are observing refractive contribution in the dark–side of the absorption. This is also true for the far–side component as can be seen in fig. 26, where we present its decomposition which shows that it is refractive although the nuclear rainbow is completely in the dark–side of the diffraction region.

VI. CONCLUSIONS

In this paper we developed a theory for the elastic scattering of strongly absorbed particles in the presence of strongly refractive mean field. Our approach starts with the absorption–free amplitude constructed from a given reasonably parametrized partial S–matrix, treated within the uniform semiclassical approximation, and, with the aid of symbol calculus, construct the absorption modified amplitude. We have shown that it is possible, within our approach, to decompose the near–side and far–side amplitudes into a well definedrefractive and diffractive components.

This further decomposition of the elastic amplitude (which can also be done within the more conventional optical potential approach as in Knoll and Schaffer[8]) is found to be quite useful in analysing intermediate energy heavy–ion elastic scattering. Application was made to the analysis of the elastic scattering data of ^{16}O off ^{40}Ca and ^{90}Zr at E_{Lab} = 1503 MeV and ^{12}C on ^{12}C and ^{12}C+^{208}Pb at E_{Lab} = 2400 MeV

APPENDIX A – CUBIC RAINBOW

In a real heavy ion scattering situation nothing prevents the deflection function from being positive for all angular momenta values and still present a minimum. In this case the nuclear rainbow angle will be positive and we will have what is known in the literature as a cubic rainbow[20], characterized by the presence of two caustics. We want to discuss in this appendix the extension of our formalism to this case. First we construct the uniform approximation for the absorption–free amplitude and then show how it can be put in an eikonal form.

We start mapping the action $2\delta(\lambda)-\lambda\theta$ onto a quartic function, i.e.,

$$2\delta(\lambda) - \lambda\theta = -\frac{\mu^4}{4} - x(\theta)\frac{\mu^2}{2} - y(\theta)\mu + A(\theta) \qquad (A.1)$$

where the fractions and the minus sign were introduced in the r.h.s. for convenience. Taking the derivative of (A.1) we see that the stationary phase points will be the roots of

$$\mu^3 + x\mu + y = 0 \quad . \qquad (A.2)$$

This is a cubic equation which has a real solution given by[17]

$$\mu_1 = s_1 + s_2 \qquad (A.3)$$

and two complex solutions

$$\mu_2 = -\frac{s_1+s_2}{2} + i\frac{\sqrt{3}}{2}(s_1-s_2) \qquad (A.4)$$

$$\mu_3 = -\frac{s_1+s_2}{2} - i\frac{\sqrt{3}}{2}(s_1-s_2) \qquad (A.5)$$

where

$$s_{1,2} = -\left[\frac{y}{2} \mp \sqrt{\Delta}\right]^{1/3} \qquad (A.6)$$

and

$$\Delta = \frac{x^3}{27} + \frac{y^2}{4} \quad . \qquad (A.7)$$

The roots $\mu_{2,3}$ are real (complex) if $\Delta \leq 0$ ($\Delta > 0$). These inequalities define in the xy plane the domains shown in fig. 28 taken from reference 21. The cusped boundary determined by the equation $\Delta = 0$ define the points where two roots are equal and corresponds to the caustics. Denoting by λ_i, with $i = 1,2,3$, the stationary angular momenta we see that the mapping is such that the domain $\Delta \leq 0$ is to be associated with the angular region between the two rainbows, namely $\theta_N \leq \theta \leq \theta_C$, where the three semiclassical trajectories contribute and, $\Delta > 0$ corresponds to $\theta < \theta_N$ and/or $\theta > \theta_C$, i.e., the shadows of the rainbows, where one complex trajectory and one real trajectory contribute.

To determine the parameters x, y and A in terms of the λ_i's we have to solve the system

$$x\mu_i^2 + 3y_i\mu_i - 4A = -4\,f_i \qquad i = 1, 2 \qquad (A.8)$$

where $f_i = 2f(\lambda_i) - \lambda_i\theta$ and we have used equation (A.1) defining the mapping and the fact that the μ_i's are the roots of Eq. (A.2) to get a simpler expression. The solution of (A.8) is an elementary but very lengthy calculation and we present here the main results. First, adding the three equations in (A.8) we obtain the relation

$$A = \frac{f_1+f_2+f_3}{3} - \frac{x^2}{6} \qquad (A.9)$$

since $\sum_i \mu_i = 0$ and $\sum_i \mu_i^2 = -2x$. After some algebraic manipulations we find that x satisfies the equation

$$x^8 - 6C_1C_2x^4 - 4(C_1^3+C_2^3)x^2 - 3(C_1C_2)^2 = 0 \qquad (A.10)$$

which is a quartic equation in x^2 and the C's are defined by

$$C_{1,2} = 2\left[\frac{f_3+f_3-2f_1}{3} \pm i\,\frac{f_2-f_3}{\sqrt{3}}\right] \quad , \qquad (A.11)$$

and y is given in terms of x by

$$y = \pm\sqrt{\frac{x^3}{27} - \frac{C_1C_2}{3x}} \quad . \qquad (A.12)$$

The positive real root of Eq. (A.10) is obtained from the standard solution, see Abramovitch and Stegun[17], as

$$x = \pm\sqrt{\sqrt{D+6C_1C_2} + \sqrt{6C_1C_2 - D + \sqrt{4D^2+48C_1C_2}}} \qquad (A.13)$$

where

$$D = \left[16(C_1^3-C_2^3)\right]^{1/3} - 2C_1C_2 \quad . \qquad (A.14)$$

This set of equations defines completely the mapping in terms of the parameters of the associated semiclassical trajectories: (A.13) together with (A.14) gives $x(\theta)$ and (A.12) and (A.9) give respectively $y(\theta)$ and $A(\theta)$. The signs of x and y are to be chosen properly.

The near–side absorption–free amplitude is now written as

$$I_0(\theta) = e^{iA} \int_{-\infty}^{\infty} d\mu \, E(\mu) \, e^{-i(\frac{\mu^4}{4} + x\frac{\mu^2}{2} + y\mu)} \qquad (A.15)$$

where $E(\mu) = \lambda^{1/2}(\mu) \frac{d\lambda}{d\mu}(\mu)$ and we have extended the inferior limit of integration to $-\infty$. Approximating $E(\mu)$ by the parabola

$$E(\mu) = p_0 + q_0\mu + r_0\mu^2 \qquad (A.16)$$

the parameters p_0, q_0 and r_0 are fixed imposing that the parabola passes through the three stationary phase points and this implies that they satisfy the system of equations

$$p_0 + q_0\mu_i + r_0\mu_i^2 = E(\mu_i) \qquad \text{with} \qquad i = 1, 2, 3 \qquad (A.17)$$

which is easily solved. On the other hand, the quantities $E(\mu)$ are calculated taking twice the derivative of (A.1) at the stationary points which yields

$$E_i = \sqrt{\frac{(3\mu_i^2 + x)\lambda_i}{-\Theta'(\lambda_i)}} \qquad i = 1, 2, 3 \; . \qquad (A.18)$$

Making use of all these relations we have just introduced, we finally have the expression of the uniform approximation for a cubic rainbow

$$I_0(\theta) = \sqrt{2\pi}\, e^{iA}\left[p_0 \bar{P}_e(x,y) + iq_0 \bar{P}'_e(x,y) - r_0 \bar{P}''_e(x,y)\right] \qquad (A.19)$$

where was defined the function

$$\bar{P}_e(x,y) = \sqrt{\frac{2}{\pi}} \int_0^{\infty} d\mu \cos y\mu \, e^{-i(\frac{\mu^4}{4} + x\frac{\mu^2}{2})} \qquad (A.20)$$

and the derivatives are with respect to y.

This function is the Pearcey function[22] and was first introduced in scattering theory and studied in numerical detail by T. Pearcey in 1946. Recently it has been studied by Trinkaus and Drepper[23] and Berry and collaborators[24] as well as da Silveira[25] in papers concerned with application of catastrophe theory to optics and quantum mechanics. In this theory the cubic rainbow is the second catastrophe known as the cusp diffraction catastrophe. The bar over the letters in (A.20) was used because the function we have obtained here is actually the complex conjugate of the standard Pearcey function.

In order to apply our method we need the Pearcey function $Pe(x,y)$ written as a sum of eikonal forms, i.e., terms containing a rapidly varying phase times a slowly varying coefficient. Based upon what we have in the case of the Airy function we observe that our Pearcey function, Eq. (A.20), as a function of y is solution of the third order differential equation

$$w''' - xw' + iyw = 0 \qquad (A.21)$$

as can be easily checked. It can also be checked that two other conjugate solutions are

$$\bar{Q}e = \sqrt{\frac{2}{\pi}} \int_0^{\infty} d\mu \cosh\left(e^{-i\frac{\pi}{8}} y\mu\right) e^{-(\frac{\mu^2}{4} - \frac{x\sqrt{i}}{2}\mu^2)} \qquad (A.22)$$

and

$$\bar{R}e = \sqrt{\frac{2}{\pi}} \int_0^{\infty} d\mu \sin y\mu \; e^{-i(\frac{\mu^4}{4} + x\frac{\mu^2}{2})} - \sqrt{\frac{2}{\pi}} \int_0^{\infty} d\mu \; e^{-i(\frac{\mu^4}{4} - x\frac{\mu^2}{2} - iy\mu)} \qquad (A.23)$$

Considering the angular region $\theta_N \leq \theta \leq \theta_C$ the three stationary points of Pearcey function itself, i.e., $\bar{P}e(x,y)$ are real and a contribute. A standard stationary phase method calculation leads us to write the formula

$$\bar{P}e(x,y) = \sum_j h_j(x,y)\ \gamma_j\ e^{i(f_j - A)} \tag{A.24}$$

for its decomposition. The factor γ_j is given by

$$\gamma_j = e^{i\ \mathrm{sgn}[\Theta'(xy)\ \frac{\pi}{4}} \tag{A.25}$$

and $h(x,y)$ is a slowly varying function of θ.

With regard to the function $\bar{Q}_e(x,y)$ we observe that its stationary values are the roots of

$$\mu^3 - x\sqrt{i}\,\mu - e^{-i\frac{\pi}{8}} y = 0 \tag{A.26}$$

which may be easily checked to be

$$\nu_i = \mu_i\, e^{-i\frac{3\pi}{8}} \tag{A.27}$$

From this we deduce using again the stationary phase method the formula

$$\bar{Q}e(x,y) = \sum_j h_j(x,y)\ \delta_j\ e^{i(f_j - A)} \tag{A.28}$$

where δ_j is given by

$$\delta_j = \begin{cases} e^{-i\frac{\pi}{8}} & \text{if} \quad \mathrm{sgn}\ \Theta'(\lambda_j) > 0 \\ e^{-i\frac{3\pi}{8}} & \text{if} \quad \mathrm{sgn}\ \Theta'(\lambda_j) < 0 \end{cases} \tag{A.29}$$

Finally the function $\bar{R}e(x,y)$ is written as

$$\bar{R}e(x,y) = \sum_j h_j(x,y)\ \gamma_j\ e^{i(\gamma_j - A - \frac{\pi}{2})}\ \mathrm{sgn}(\mu_j)\ . \tag{A.30}$$

The three equations (A.24), (A.28) and (A.30) define the functions $h_j(x,y)$ since given the Pearcey functions they may be inverted to give the h's. Similar relations may be derived for the derivatives. The difference will be in the factors γ and δ which will appear to the square and cubic power for the first and second derivative respectively. Outside the angular region between the rainbow, that is, the domain limited by the caustics, only two stationary points, one real and one complex, and two functions, $\bar{P}e(x,y)$ and $\bar{Q}e(x,y)$, have to be considered. This ends this Appendix. As a last comment we say that numerical investigation of these formulas and application to heavy ion system are in progress.

APPENDIX B – RELATION OF THE PHASE SHIFT TO THE PARAMETERS OF THE OPTICAL POTENTIAL

To do numerical calculations and data analysis with the scattering formalism we developped in this paper, we have to assume some specific form of the S–matrix. One way of doing this, is to parametrize directly the S–matrix elements, leaving aside the question of how they are generated. The vast majority of researchers, however, use the conventional data–fitting with a parametrized optical potential. The purpose of this Appendix is to supply to the optical potential practioners simple analytical relations between the partial elastic element of the S–matrix and the corresponding optical potential. For strongly absorbing potentials Kauffmann[26] has derived analytic expressions, for the reflection function and the nuclear phase shift, valid for very heavy ions, that is, strong Coulomb interaction. These are not the conditions we are interested in. Indeed, since we want to investigate the nuclear rainbow, we have to suppose relatively transparent potentials and weak Coulomb interaction. In the following we discuss two methods for relating S_ℓ to the optical potential which have been widely used in the literature.

B.1. THE KNOLL–SCHAEFFER METHOD

Our starting pont is the eikonal approximation, as it was modified by Knoll and Schaeffer[8] for nuclear potentials of the Woods–Saxon form, i.e.,

$$V_N = -Vf(x_r) - iWf(x_i) \quad , \quad f(x) = (e^x+1)^{-1}$$
$$x_{r,i} = \frac{r - R_{r,i}}{a_{r,i}} \tag{B.1}$$

with small diffusenesses $a_{r,i} \ll R_{r,i}$. Their expression for the nuclear phase shift can be written as

$$2\delta^N(r_0) = \frac{k}{E}\sqrt{2r_0}\left[V\sqrt{a_r}\,g(x_r) + iW\sqrt{a_i}\,g(x_i)\right] \tag{B.2}$$

where

$$g(x) = \int_0^\infty \frac{dv}{\exp(x+v)^2 + 1} \tag{B.3}$$

and r_0 is the turning point.

It will be shown to be convenient to obtain approximate closed form for the function $g(x)$. To do this, we consider first the case $x \geq 0$, where the most important contribution to the integral comes from the vicinity of $v=0$. We can then replace the integrand by the expansion

$$(\exp(x+v^2)+1)^{-1} = e^{-\ln(1+e^{(x+v^2)})}$$
$$= \exp\left[-\left[\ln(1+e^x) + \frac{e^x}{e^x+1}v^2 + \cdots\right]\right] . \tag{B.4}$$

Integrating Eq. (B.3) and keeping only the first two terms, we get

$$g(x) = \frac{\exp(x/2)}{\sqrt{\exp(x)+1}}\sqrt{\frac{\pi}{2}} \quad , \quad x \geq 0 \tag{B.5}$$

For $x \leq 0$, we divide the integration interval into the intervals $(0, \sqrt{-x})$ and $(\sqrt{-x}, \infty)$, and rewrite $g(x)$ as

$$g(x) = \int_0^{\sqrt{-x}} dv - \int_0^{\sqrt{-x}} \frac{dv}{e^{-x-v^2}+1} + \int_{\sqrt{-x}}^\infty \frac{dv}{e^{x+v^2}+1} . \tag{B.6}$$

The first integral is immediately performed. In the second and third integrals we use,

respectively, the expansions

$$\left[\exp(-(x+v^2)) + 1\right]^{-1} = \exp\left[-(\ln 2 - \sqrt{-x}\,(v-\sqrt{-x}\,) + \cdots\right] \tag{B.7}$$

and

$$\left[\exp(x+v^2) + 1\right]^{-1} = \exp\left[-(\ln 2 + \sqrt{-x}\,(v-\sqrt{-x}\,) + \tfrac{1}{2}(1-x)(v-\sqrt{-x}\,)^2 + \cdots\right] \tag{B.8}$$

about $v = \sqrt{-x}$. Neglecting the higher order terms we find

$$g(x) \simeq \sqrt{-x} - \frac{1 - e^x}{2\sqrt{-x}} + \frac{e^{u^2}}{\sqrt{2(1-x)}}\sqrt{\frac{\pi}{2}}\,\mathrm{erfc}(u) \quad , \quad x \le 0 \tag{B.9}$$

where $u = \sqrt{\frac{-x}{2(1-x)}}$. We observe that for negative x, u is smaller than unity which is its limit for $x \to -\infty$. Thus we can put $\mathrm{erfc}(u) \simeq 1 - u\,e^{-u^2}$ in Eq. (B.9), obtaining a simpler expression for $g(x)$. This equation shows that $g(x)$ behaves, for large negative values of x, as $\sqrt{-x}$.

Eq. (B.9) together with Eq. (B.5) form a continuous representation of $g(x)$. However, it is not a differentially continuous functions at $x=0$. This fact renders Eq. (B.9) not quite appropriate for the obtention of the deflection function (the derivative of $2\delta^N$. Eq. (B.2)). To remedy this situation, we present below an alternative approximation to $g(x)$, which is more adequate.

The idea is to divide the integration interval about the point at which the integrand has a point of inflexion. Designating this point by $\bar{v}$, it is easy to show that it is given by the solution of the transcendental equation

$$\bar{v}^2 = \tfrac{1}{2}\coth\left[\frac{x + \bar{v}^2}{2}\right] \quad . \tag{B.10}$$

Proceeding now as we did to deduce Eq. (B.9) we obtain, after some algebra, the equation

$$g(x) \simeq \bar{v} - \frac{\mu}{2\bar{v}}\left[1 - e^{-\frac{2\bar{v}^2}{\mu+1}}\right] + \frac{e^{\mu/2}}{\bar{v}\sqrt{2\mu}}\,\mathrm{erfc}\left[\sqrt{\frac{\mu}{2}}\right]\sqrt{\frac{\pi}{2}} \tag{B.11}$$

valid for any x and where $\mu = \exp(x+\bar{v}^2)$.

To compare the behaviour of Eq. (B.11) above with the approximation to $g(x)$ obtained before, we observe first that the solution of the transcendental equation goes to

$$\bar{v} \simeq \sqrt{-x} \tag{B.12}$$

when $-x \gg 1$ and therefore Eq. (B.11) must go to Eq. (B.9). On the other hand for great positive values of x, the solution of Eq. (B.10) goes to

$$\bar{v} \simeq \frac{1}{\sqrt{2}} \quad . \tag{B.13}$$

Since when $x \gg 1$, $\mu \gg 1$, we can neglect the factor 1 in the exponential of the second term in the r.h.s. of Eq. (B.11). Expanding the exponential up to third order in $1/\mu$ we obtain $\mathrm{erfc}(y) \simeq \frac{2}{\sqrt{\pi}}\frac{e^{-y^2}}{2y}$,

$$g(x) \simeq \sqrt{\frac{2}{e}}\,e^{-x} \tag{B.14}$$

which should compare with Eq. (B.5). In fact, for $x \gg 1$, this equation gives an exponential form for $g(x)$, while the factor $\frac{\sqrt{\pi}}{2} \simeq \sqrt{\frac{2}{e}}$.

Eq. (B.11) with $\bar{v}$ given by Eq. (B.10), is analytical and so can be derived in order to find an approximate expression for $g(x)$. A somewhat lengthy calculation yields

$$g'(x) \simeq \left\{1-\frac{\mu}{2\bar{v}}\left[a-\frac{1}{\bar{v}}\right]\left[1-\left[e^{-\frac{2\bar{v}^2}{\mu+1}}\right]\right]+\frac{\mu}{\mu+1}\left[2-\frac{a}{\mu+1}\right]\exp\left[-\left[\frac{2\bar{v}^2}{\mu+1}\right]\right]+\right.$$

$$\left.+\left[a\left[\frac{\mu}{2}-1\right]-\frac{1}{\bar{v}}\right]\frac{e^{\mu/2}}{\bar{v}\sqrt{2\mu}}\sqrt{\frac{\pi}{2}}\ \mathrm{erfc}\left[\sqrt{\frac{\mu}{2}}\right]-\frac{a}{4\bar{v}}\right\}\bar{v}' \qquad (B.15)$$

where

$$\bar{v}' = \frac{1-4\ \bar{v}^4}{6+8\ \bar{v}^4} \qquad (B.16)$$

and

$$a = 1+2\,\bar{v}\bar{v}' = \frac{4}{3+4\bar{v}^4}\ . \qquad (B.17)$$

Eq. (B.15) can now be inserted in the expression

$$\Theta^{(N)}(r_0) = -\left[\frac{Vg'(x_r)}{\sqrt{a_r}}+\frac{iWg'(x_i)}{\sqrt{a_i}}\right]\sqrt{2r_0} \qquad (B.18)$$

for the derivative of the phase shift. A comparison of our approximation for the deflection function and the profile function is shown in figures 29 and 30..

As an application of the relations above, it is interesting to observe that we can extract from them an approximate expression for the slope of the exponential shadow of the nuclear rainbow, given by the imaginary part of the turning point, in terms of the parameters of the optical potential.

To do this we observe that since the nuclear rainbow occurs at negative values of the variable x, we can take

$$g(x) \simeq \bar{v} \qquad (B.19)$$

and approximate Eq. (81) by the equation

$$\bar{v}^2(x+\bar{v}^2) \simeq 0 \qquad (B.20)$$

whose solution can be written as

$$\bar{v} = \exp\left[-\frac{1}{2}\sinh^{-1}\frac{x}{2}\right]\ . \qquad (B.21)$$

Supposing equal geometry we obtain the deflection function

$$\Theta^N(r_0) \simeq -\frac{|V+iW|}{4E}\sqrt{\frac{2R}{a}}\ \frac{e^{i\phi}\ \exp\left[-\frac{1}{2}\sinh^{-1}\left[\frac{r_0-R}{2a}\right]\right]}{\sqrt{1+\left(\frac{r_0-R}{2a}\right)^2}} \qquad (B.22)$$

with $\phi = \tan^{-1}(W/V)$. This equation shows that real solutions are obtained when

$$\mathrm{Im}\ r_0 \cong \frac{2aWV}{W^2+V^2}\ . \qquad (B.23)$$

B.2. THE KAROL METHOD

Taking a microscopic view of the optical potential based on multiple scattering theory, the ion–ion interaction is then constructed as a "$t\rho_1\rho_2$". Karol[27] parametrizes the densities as Gaussians, which allows an analytic construction of the potential when cylindrical coordinates are employed. The potential is found to have the form

$$V_{AB} = -\left\langle t_{NN}(E_{NN})\right\rangle 2\pi^{3/2}\,\rho_A(0)\,\rho_B(0)\,\frac{a_A^3 a_B^3}{(a_A^2+a_B^2)^{3/2}}\ \exp\left[\frac{-z^2-b^2}{a_A^2+a_B^2}\right] \qquad (B.24)$$

where the a,s are the Gaussian widths and $\rho_A(0)$ and $\rho_B(0)$ are the central densities. $\left\langle t_{NN}(E)\right\rangle$ is the average nucleon–nucleon t–matrix in the forward direction.

The relation between the density parameters $\rho(0)$ and a and the corresponding

ones of the conventional Fermi–function form of ρ is discussed in details in Karol and we shall not repeat it here.

Within Glauber approximation, the elastic nuclear S–matrix is given by

$$S_{\ell(b)} = \exp\left[-\frac{k\,i}{2E}\int_{-\infty}^{\infty} V_{AB}(b,z')\,dz'\right] \qquad (B.25)$$

where k (asymptotic wave number) and E (center of mass energy) refer to the ion–ion system. The integration in B.25 is straightforward and gives

$$S_{\ell(b)} = \exp\left\{+\frac{k\,i}{2E}\left\langle t_{NN}(E_{NN})\right\rangle \pi^2\,\rho_A(0)\,\rho_B(0)\,\frac{a_A^3\;a_B^3}{a_A^2+a_B^2}\,\exp\left[-\frac{b^2}{a_A^2+a_B^2}\right]\right\} \qquad (B.26)$$

Writing $\quad \mathrm{Re}\,t = \alpha(E)\,\mathrm{Im}\,t$

and
$$\langle \mathrm{Im}\,t\rangle = -4\pi\frac{E}{k^2}\,\frac{k}{4\pi}\langle\sigma_{NN}(E)\rangle$$
$$= -\frac{E}{k}\langle\sigma_{NN}(E)\rangle \qquad (B.27)$$

where α is a known function of energy, we have finally for the reflection coefficient

$$|S_b| = \exp\left[-A\exp\left[-\frac{b^2}{a_A^2+a_B^2}\right]\right] \qquad (B.28)$$

and the phase

$$2\delta = \alpha\,A\exp\left[-\frac{b^2}{a_A^2+B_A^2}\right]$$

$$A = \frac{\sigma_{NN}(E)}{2}\,\pi^2\,\rho_A(0)\,\rho_B(0)\,\frac{a_A^3\;a_B^3}{a_A^2+a_B^2}\;. \qquad (B.29)$$

The above expressions are quite simple and contain no free parameter. They have been used by Chauvin et al.[28] to analyse the $^{12}C+^{12}C$ elastic scattering at E/A = 25, 30 and 85 MeV.

REFERENCES

1) See, e.g., R.C. Fuller, *Phys. Rev.* **C12** (1975) 1561: for a recent review see, M.S. Hussein and K.W. McVoy, *Prog. Part. Nucl. Phys.* **12** (1984) 103.

2) W.E. Frahn, "*Diffractive Processes in Nuclear Physics*" (Oxford University Press 1985).

3) W.E. Frahn and D.H.E. Gross, *Ann. Phys.* (NY) **101** (1976) 520.

4) H.G. Bohlen, X.S. Chen, J.M. Cramer, P. Fröhlich, B. Gebauer, H. Lettau, A. Miczaika, W. von Oertzen, R. Ulrich and T. Wilpert, *Z. Phys.* **A332** (1985) 241.

5) S.H. Fricke and K.W. McVoy, *Nucl. Phys.* **A467** (1987) 291.

6) M.E. Brandan, S.H. Fricke and K.W. McVoy, *Phys. Rev.* **C38** (1988) 673; S.H. Fricke, M.E. Brandan and K.W. McVoy, *Phys. Rev.* **C38** (1988) 682; S.H. Fricke, P.J. Hatchell, K.W. McVoy and G.R. Satchler, Mad/NT/89–03.

7) E. Vigezzi and A. Winther, NBI–88–82.

8) J. Knoll and R. Schaeffer, *Ann. Phys.* (NY) **97** (1976) 307.

9) R. da Silveira, Orsay preprint, IIPNO/TH88–69.

10) M.V. Berry, *Proc. Phys. Soc.* **89** (1966) 479; M.V. Berry and E.K. Mount, *Rep. Prog. Phys.* **35** (1972) 315.

11) V.P. Maslov and M.V. Fedoriuk, "*Semiclassical Approximation in Quantum Mechanics*" (Riedel, Dorderchet 1981).

12) M.P. Pato and M.S. Hussein, *Phys. Lett.* **207** (1988) 121.

13) M.S. Hussein and M.P. Pato, *Mod. Phys. Lett.* **A3** (1988) 469.

14) S.W. McDonald, *Phys. Rep.* **158** (1988) 337.

15) R. da Silveira, *Z. Phys.* **A299** (1981) 79.

16) C. Chester, B. Friedman and F. Ursell, *Proc. Camb. Phil. Soc.* **53** (1957) 599.

17) M. Abramowitz and I.A. Stegun, *Handbook of Mathematical Functions* (Dover, New York, 1970).

18) M.C. Mermaz, *Z. Phys.* **A321** (1985) 613.

19) M.C. Mermaz, B. Bonin, M. Buenerd and J.Y. Hostachy, *Phys. Rev.* **C34** (1986) 1988.

20) J.N. Conner and M.S. Child, *Molecular Phys.* **18** (1970) 653.

21) F.J. Wright, *J. Phys.* **A13** (1980) 2913.

22) T. Pearcey, *Phil. Mag.* **37** (1946) 311.

23) H. Trinkaus and F. Drepper, *J. Phys.* **A10** (1977) L11.

24) M.V. Berry and M.R. Mackley, *Phil. Trans. R. Soc.* **A287** (1977) 1; M.V. Berry, J.F. Nye and F.J. Wright, *Phil. Trans. R. Soc.* **A291** (1979) 453.

25) R. da Silveira, *Z. Phys.* **A299** (1981) 79.

26) S.K. Kauffmann, Univ. of Cape Town preprints (1976), umpublished. See Ref. (2) for some details.

27) P.J. Karol, *Phys. Rev.* **C11** (1975) 1203.

28) J. Chauvin, D. Lebrun, A. Lounis and M. Buenerd, *Phys. Rev.* **C28** (1983) 1970.

TABLE I. Mc Intyre's phase shift parameters

System	$^{16}O+^{40}Ca$	$^{16}O+^{90}Zr$	$^{12}C+^{12}C$	$^{12}C+^{208}Pb$
A	183.041	244.132	73.89	351.78
Δ	20.271	17.080	13.86	37.09
d_1	4.404	3.331	0.5686	3.0412
A_1	133.873	206.410	80.11	253.08
Δ_1	15.519	21.774	14.49	28.95

FIGURE CAPTIONS

Fig. 1 – Coefficients and phases of the Airy function and its derivative as a function of the argument x.

Fig. 2 – Comparison between the exact cross section given by the partial wave sum (full line) and the cross section calculated with our semiclassical formalism (dashed line) for an illustrative example. The absorption–free cross section is also shown (dotted line).

Fig. 3 – The same as fig. 2 for the near– and the far–side separately.

Fig. 4 – Decomposition of the near–side cross section in its diffractive (D) and refractive subcomponents, rainbow (R) and internal trajectory (IT). The near–side absorption–free cross section is also shown.

Fig. 5 – Decomposition of the far–side cross section and the far–side absorption–free cross section.

Fig. 6 – The deflection function (full line) and the profile function (dotted line) for the example discussed in the preceding figures.

Fig. 7 – Fitting of the data using a McIntyre parametrization of the S–matrix.

Fig. 8 – The same of Fig. 7.

Fig. 9 – The same of Fig. 7.

Fig. 10 – The total semiclassical cross section and its near (N) and far (F) components for the system $^{16}O+^{40}Ca$. The triangle dots are exact cross section given by the partial wave sum.

Fig. 11 – The near–side semiclassical cross section of the system $^{16}O+^{40}Ca$ (N) and its diffractive (D), rainbow (R) and internal trajectory (IT) subcomponent.

Fig. 12 – The far–side semiclassical cross section (F) of the system $^{16}O+^{40}Ca$ and its diffractive (D) and rainbow (R) subcomponent.

Fig. 13 – Path in the complex plane of the angular momenta of the complex trajectories in the shadow of the coulomb and nuclear rainbow for the system $^{16}O+^{40}Ca$. Also shown are the first poles of the deflection and profile functions.

Fig. 14 – Deflection (full line) and profile function (dotted line) of the system $^{16}O+^{40}Ca$.

Fig. 15 – Total (full line), near (N), far (F) and exact (triangle dots) cross sections for the system $^{16}O+^{90}Zr$.

Fig. 16 – Diffractive (D), rainbow (R) and internal trajectory (IT) components of the near–side (N) $^{16}O+^{90}Zr$ cross section.

Fig. 17 – Decomposition of the far–side cross section of $^{16}O+Zr$.

Fig. 18 – The same as fig. 13 for $^{16}O+^{90}Zr$.

Fig. 19 – Deflection function (full line) and profile function (dotted line) for $^{16}O+^{90}Zr$.

Fig. 20 – Exact cross section (triangle dots) and near–far decomposition for the system $^{12}C+^{12}C$.

Fig. 21 – Refractive–diffractive decomposition of the near–side cross section of $^{12}C+^{12}C$.

Fig. 22 – Refractive–diffractive decomposition of the far–side cross section of $^{12}C+^{12}C$.

Fig. 23 – Deflection and profile function for $^{12}C+^{12}C$.

Fig. 24 – Exact cross section and near–far decomposition for the system of $^{12}C+^{208}Pb$.

Fig. 25 – Decomposition of the near–side cross section of $^{12}C+^{208}Pb$.

Fig. 26 – Decomposition of the far–side cross section of $^{12}C+^{208}Pb$.

Fig. 27 – Deflection and profile function for $^{12}C+^{208}Pb$.

Fig. 28 – The three region of the (x,y) plane in which the stationary phase points behave differently.

Fig. 29 – Comparison of the approximation for the modulus of the S–matrix with the optical model output.

Fig. 30 – The same as fig. 29 for the deflection function.

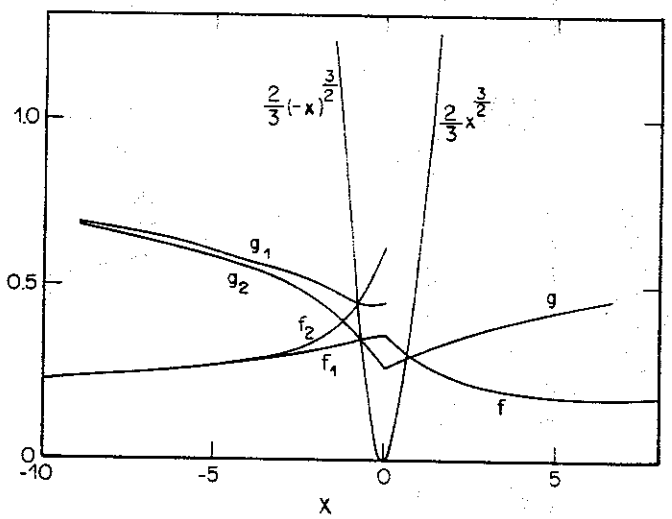
1.0
0.5
0
-10
-5
0
5
X
$\frac{2}{3}(-x)^{\frac{3}{2}}$
$\frac{2}{3}x^{\frac{3}{2}}$
g_1
g_2
f_2
f_1
g
f

1

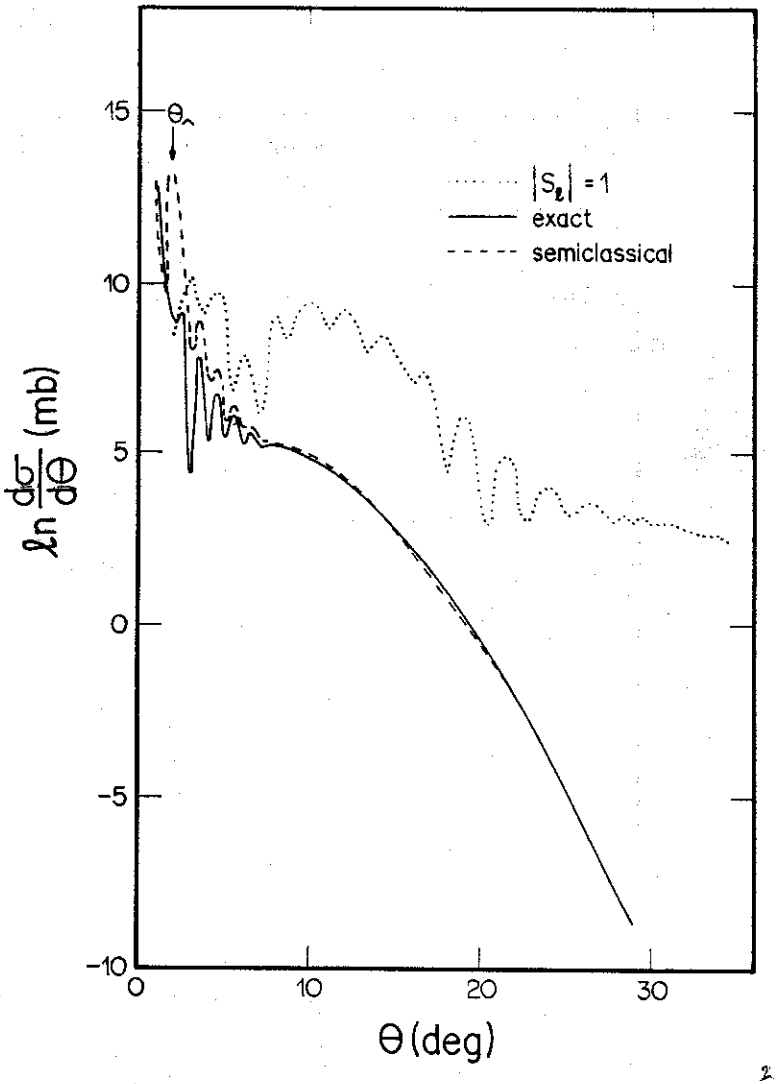
15
10
5
0
-5
-10
0
10
20
30
θ
$|S_\ell| = 1$
exact
semiclassical
$\ell n \frac{d\sigma}{d\Theta}$ (mb)
Θ (deg)

2

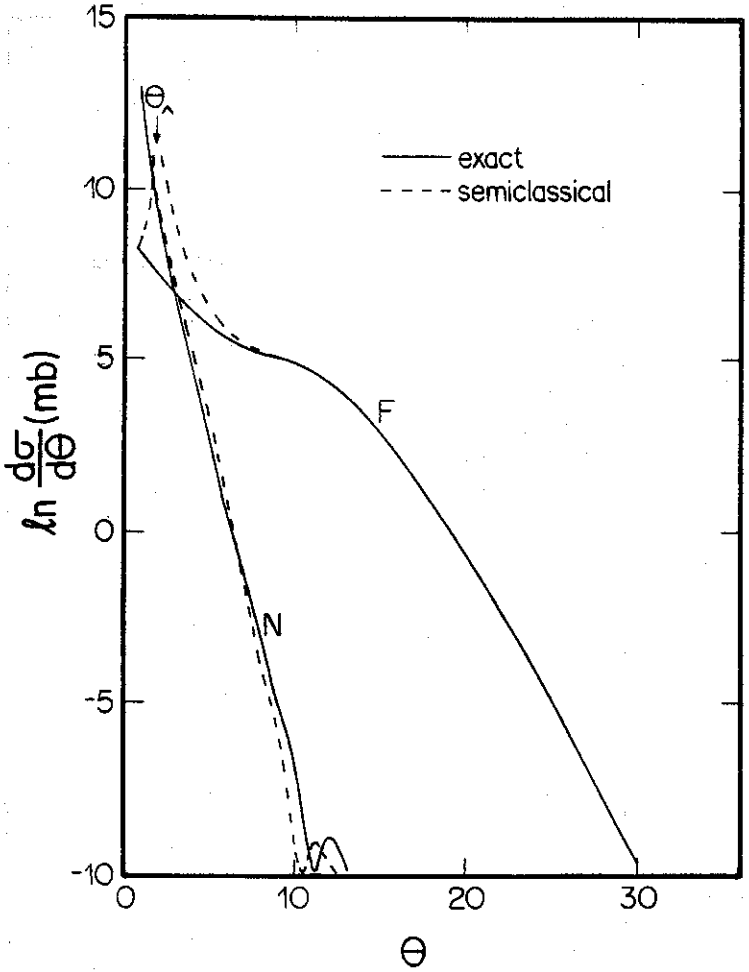
15
10
5
0
-5
-10
0
10
20
30
Θ
ℓn dσ/dΘ (mb)
Θ
exact
semiclassical
F
N

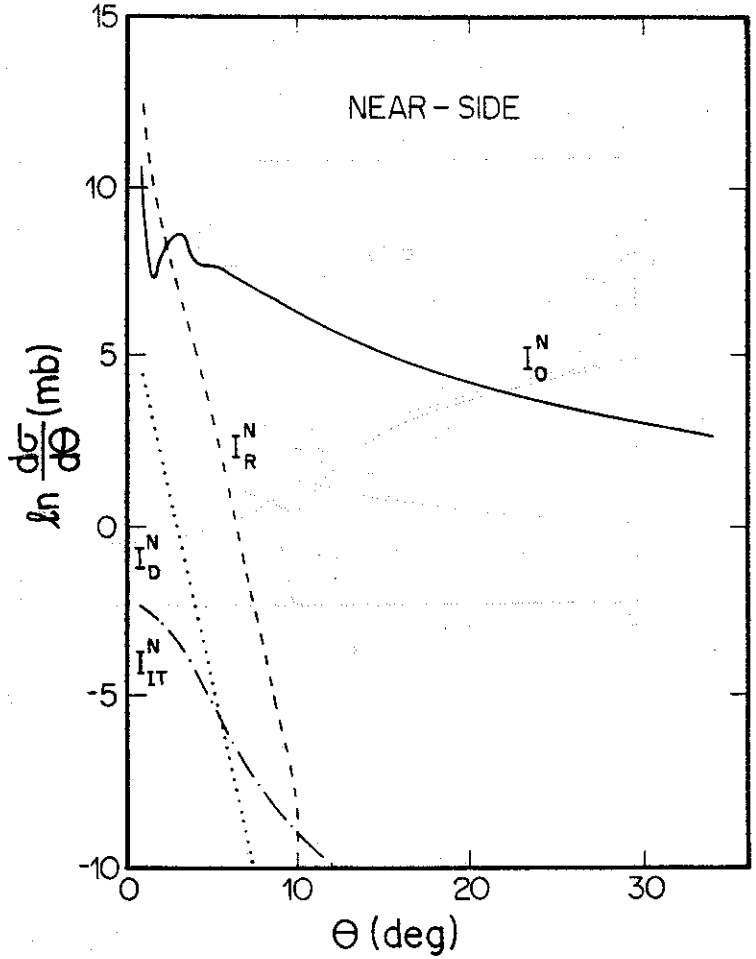
15
10
5
0
-5
-10
0
10
20
30
Θ (deg)
ℓn dσ/dΘ (mb)
NEAR – SIDE
I_O^N
I_R^N
I_D^N
I_{IT}^N

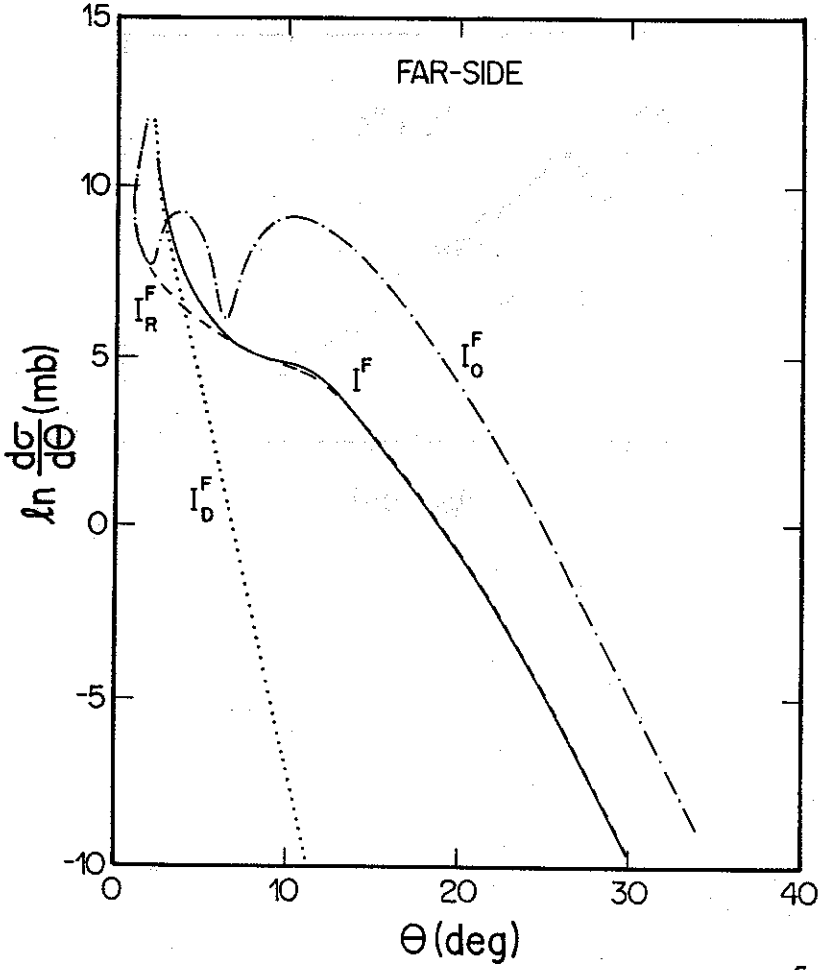
FAR-SIDE
15
10
5
0
-5
-10
0
10
20
30
40
$\ell n \frac{d\sigma}{d\Theta}$ (mb)
Θ (deg)
I_R^F
I_D^F
I^F
I_o^F

5

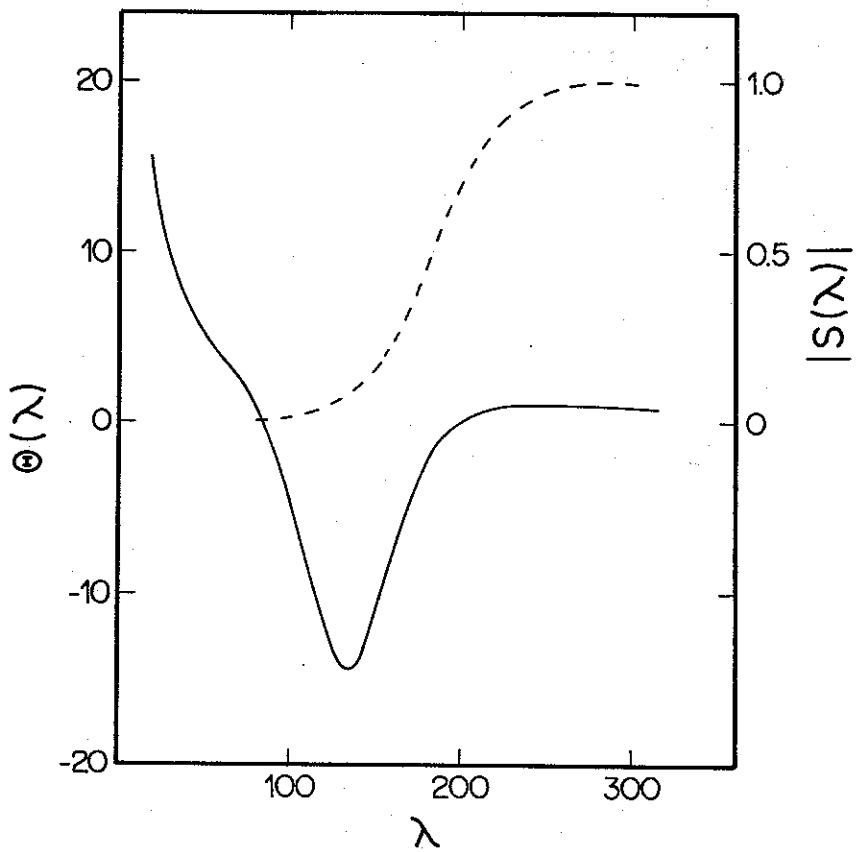
20
10
0
-10
-20
100
200
300
λ
$\Theta(\lambda)$
1.0
0.5
0
$|S(\lambda)|$

6

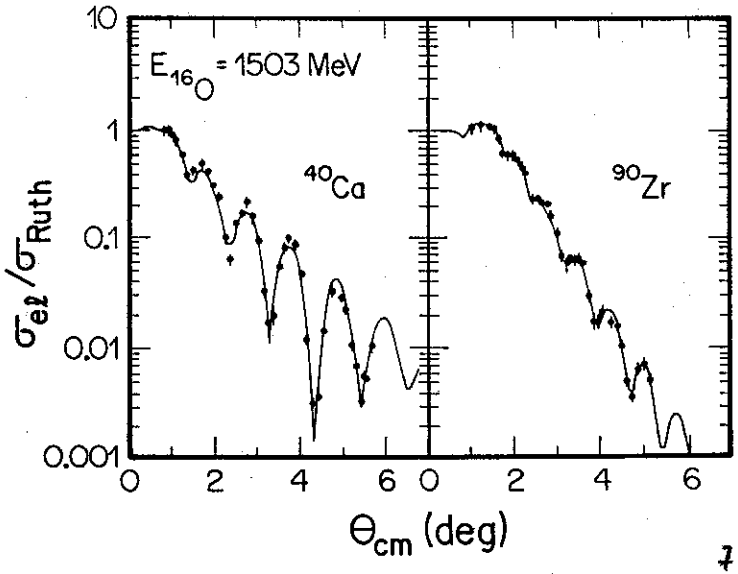
$E_{^{16}O}$ = 1503 MeV
^{40}Ca
^{90}Zr
$\sigma_{el}/\sigma_{Ruth}$
Θ_{cm} (deg)

7

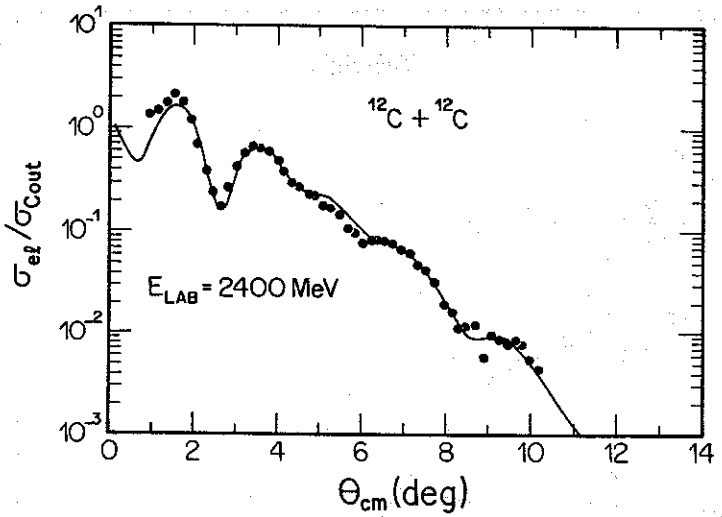
$^{12}C + ^{12}C$
E_{LAB} = 2400 MeV
$\sigma_{el}/\sigma_{Cout}$
Θ_{cm} (deg)

8

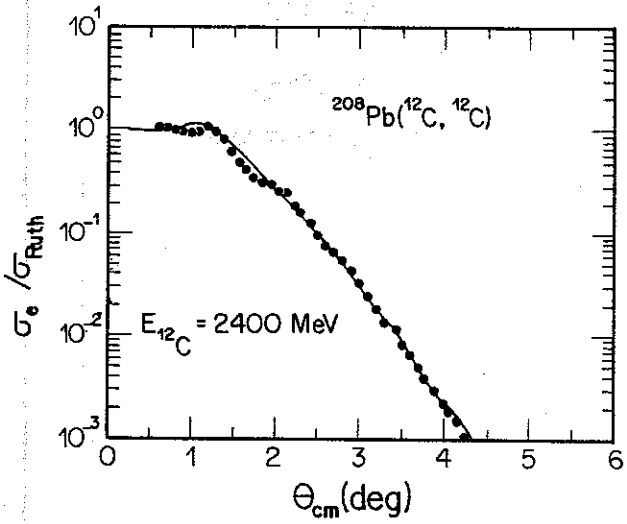
10^1
10^0
10^{-1}
10^{-2}
10^{-3}
σ_e / σ_{Ruth}
$^{208}Pb(^{12}C, ^{12}C)$
$E_{^{12}C}$ = 2400 MeV
0 1 2 3 4 5 6
Θ_{cm}(deg)

9

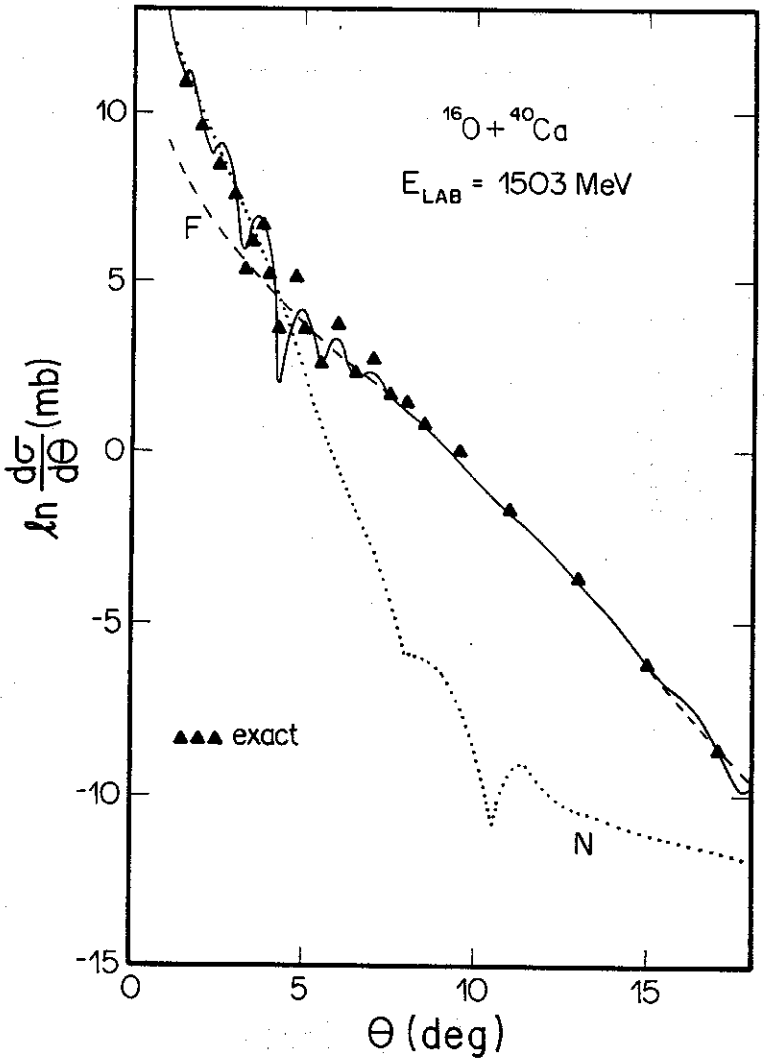
$^{16}O + ^{40}Ca$
E_{LAB} = 1503 MeV
F
N
▲▲▲ exact
10
5
0
-5
-10
-15
0 5 10 15
$\ell n \frac{d\sigma}{d\Theta}$(mb)
Θ (deg)

10

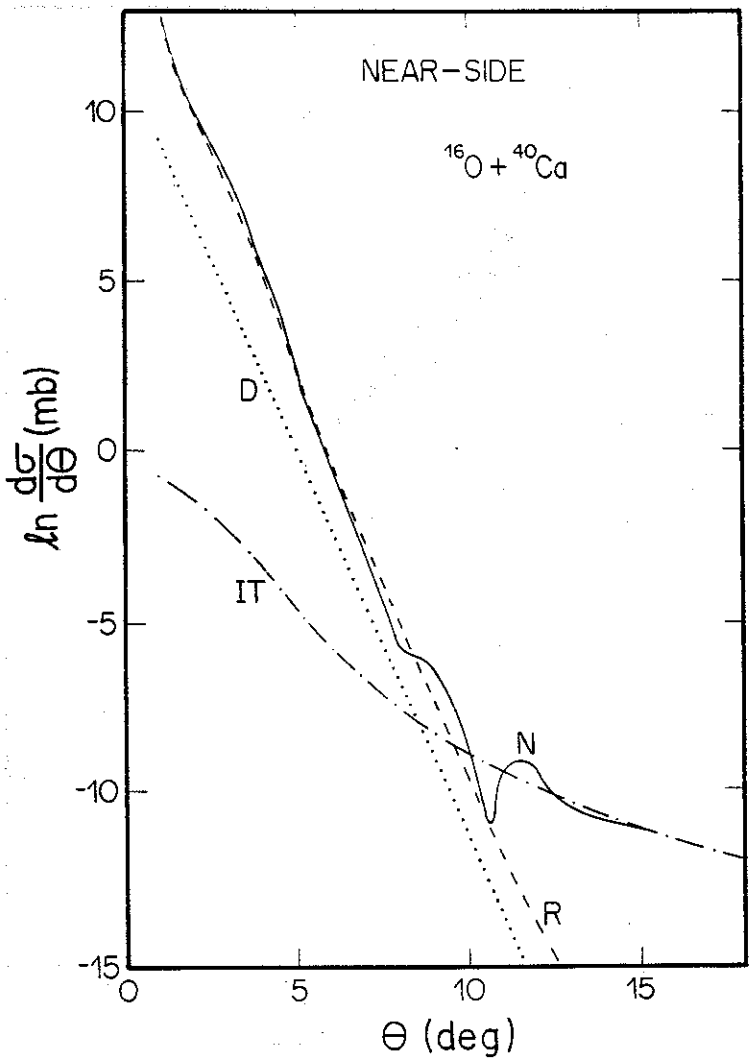
NEAR-SIDE
$^{16}O + ^{40}Ca$
D
IT
N
R
10
5
0
-5
-10
-15
0
5
10
15
$\ell n \frac{d\sigma}{d\Theta}$ (mb)
Θ (deg)

11

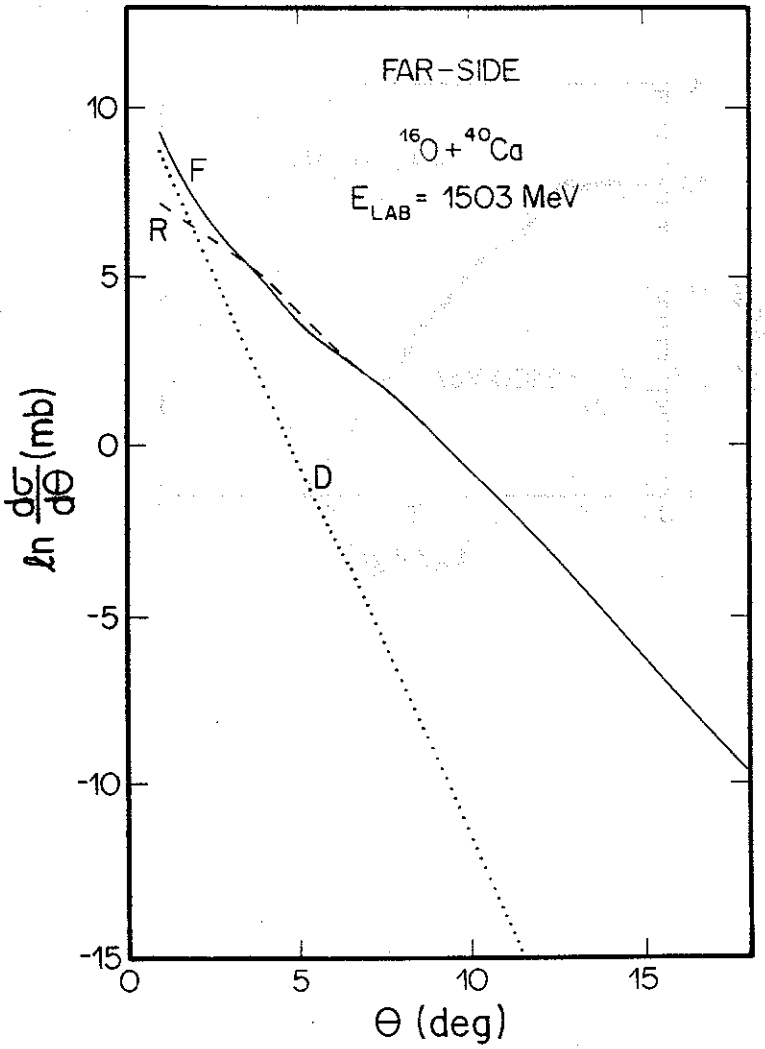
FAR-SIDE
$^{16}O + ^{40}Ca$
E_{LAB} = 1503 MeV
F
R
D
10
5
0
-5
-10
-15
0
5
10
15
$\ell n \frac{d\sigma}{d\Theta}$ (mb)
Θ (deg)

12

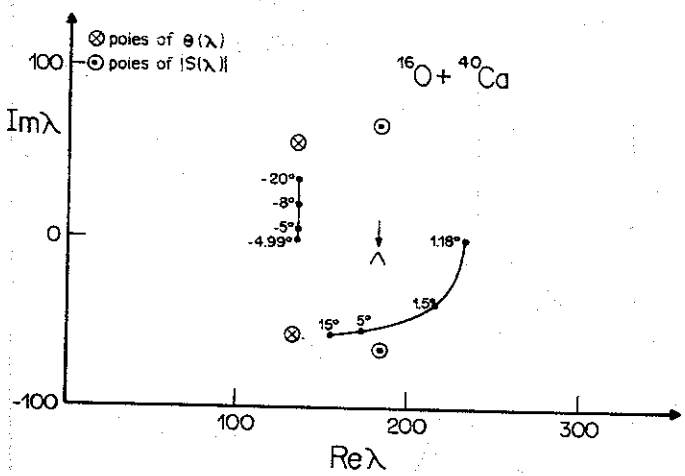
⊗ poles of θ(λ)
⊙ poles of |S(λ)|
$^{16}O + ^{40}Ca$
Imλ
Reλ
100
0
-100
100
200
300
-20°
-8°
-5°
-4.99°
1.18°
1.5°
15°
5°

13

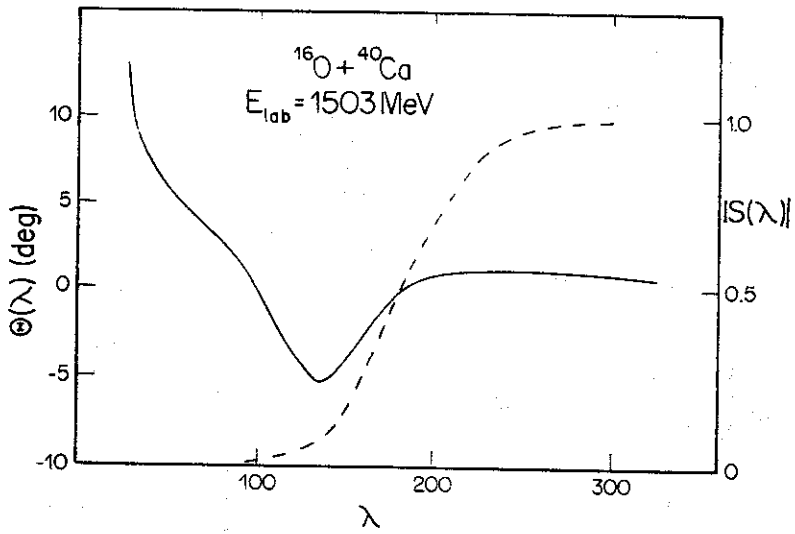
$^{16}O + ^{40}Ca$
$E_{lab} = 1503$ MeV
Θ(λ) (deg)
|S(λ)|
λ
10
5
0
-5
-10
1.0
0.5
0
100
200
300

14

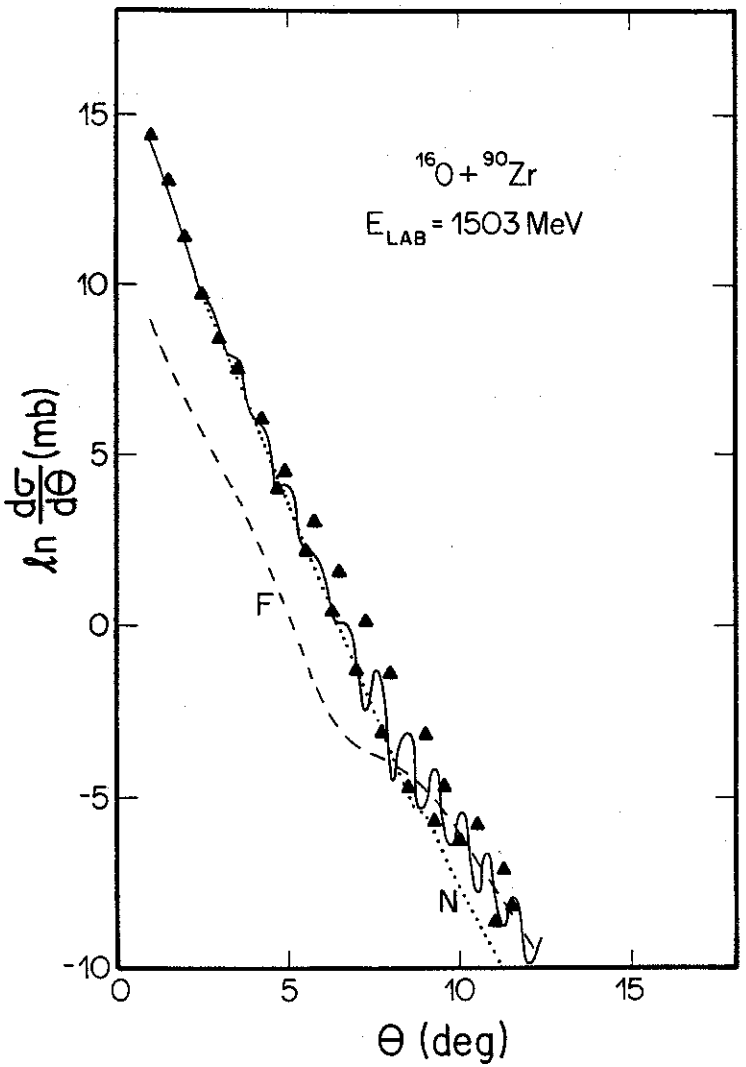
$^{16}O + ^{90}Zr$
E_{LAB} = 1503 MeV
F
N
$\ln \frac{d\sigma}{d\Theta}$(mb)
Θ (deg)
15
10
5
0
-5
-10
0
5
10
15

15

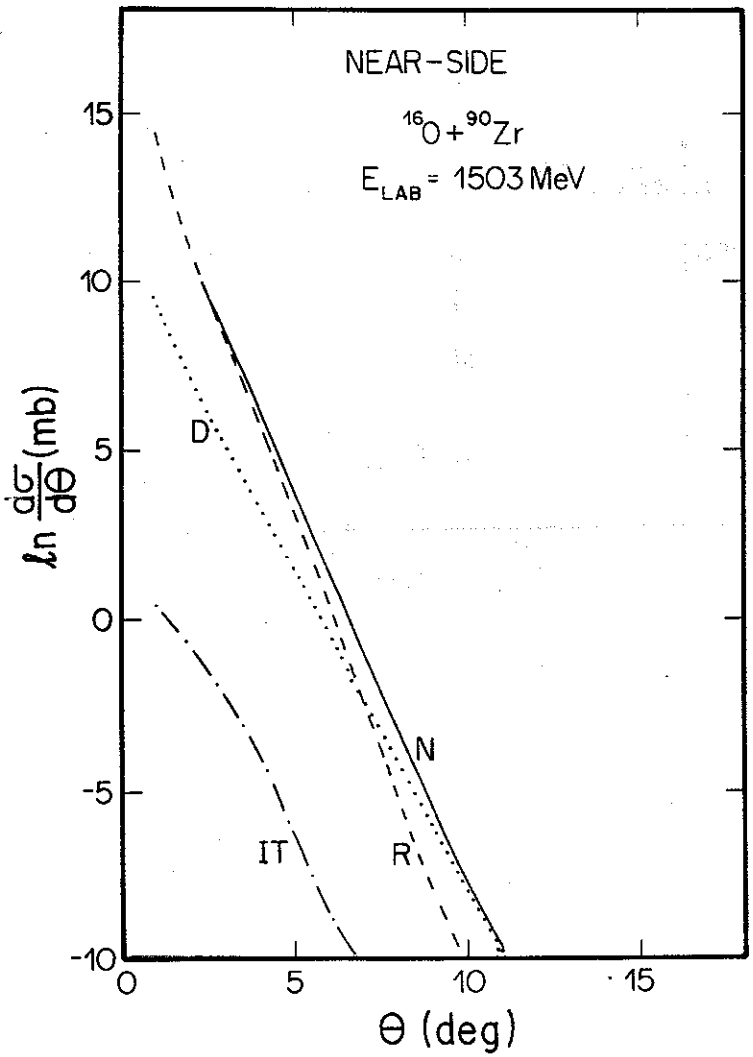
NEAR-SIDE
$^{16}O + ^{90}Zr$
E_{LAB} = 1503 MeV
D
N
IT
R
$\ln \frac{d\sigma}{d\Theta}$(mb)
Θ (deg)
15
10
5
0
-5
-10
0
5
10
15

16

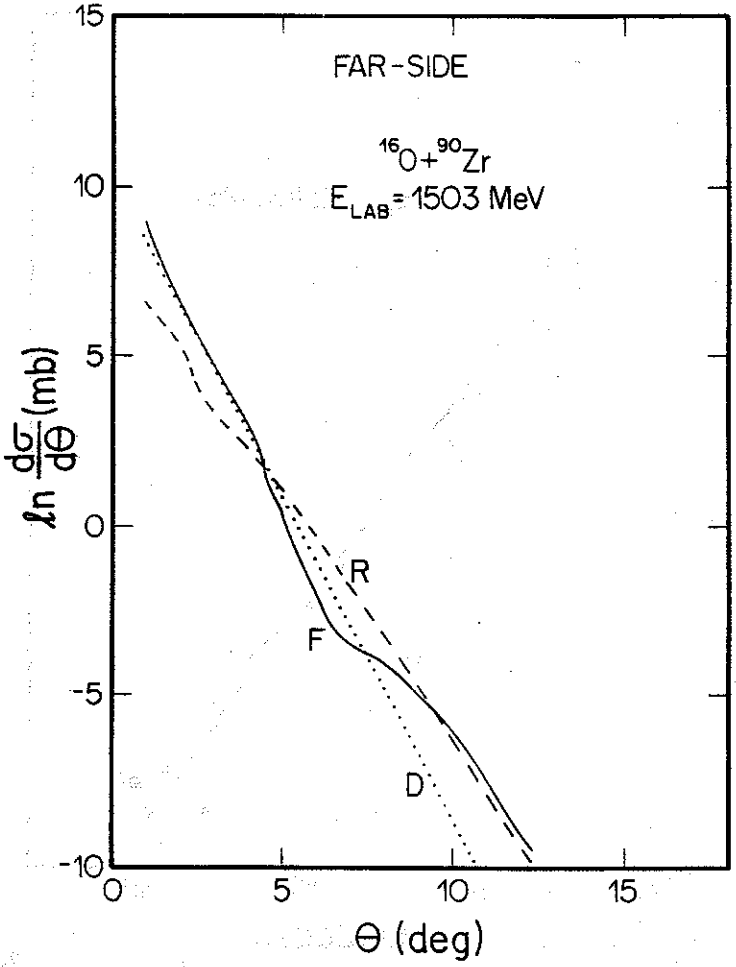
FAR-SIDE
$^{16}O+^{90}Zr$
E_{LAB} = 1503 MeV
R
F
D
$\ell n \frac{d\sigma}{d\Theta}$ (mb)
Θ (deg)
15
10
5
0
-5
-10
0
5
10
15

17

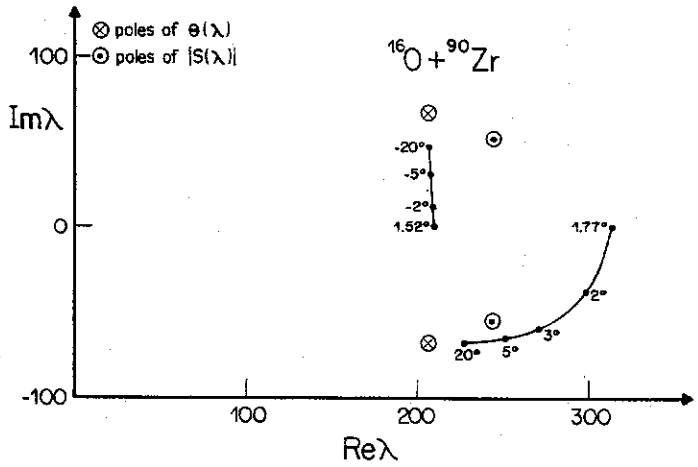
⊗ poles of θ(λ)
⊙ poles of |S(λ)|
$^{16}O+^{90}Zr$
Imλ
Reλ
100
0
-100
100
200
300
-20°
-5°
-2°
1.52°
1.77°
2°
3°
5°
20°

18

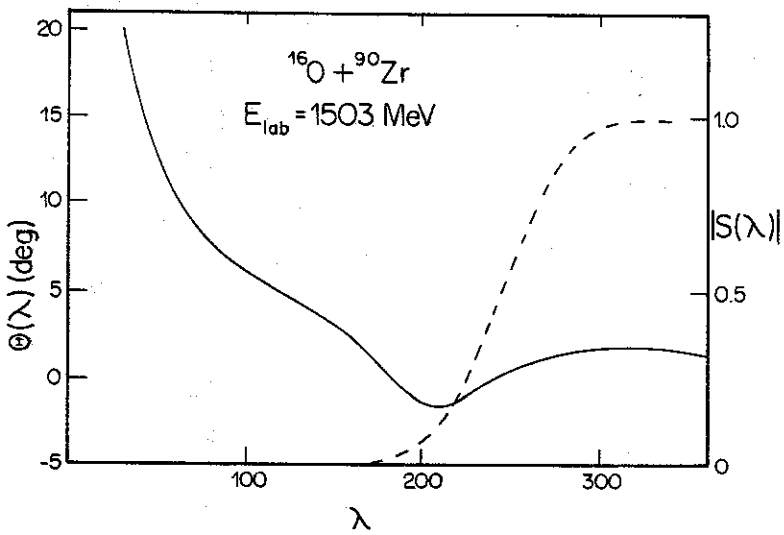
$^{16}O + ^{90}Zr$
$E_{lab} = 1503$ MeV
$\Theta(\lambda)$ (deg)
$|S(\lambda)|$
λ
20
15
10
5
0
-5
1.0
0.5
0
100
200
300

19

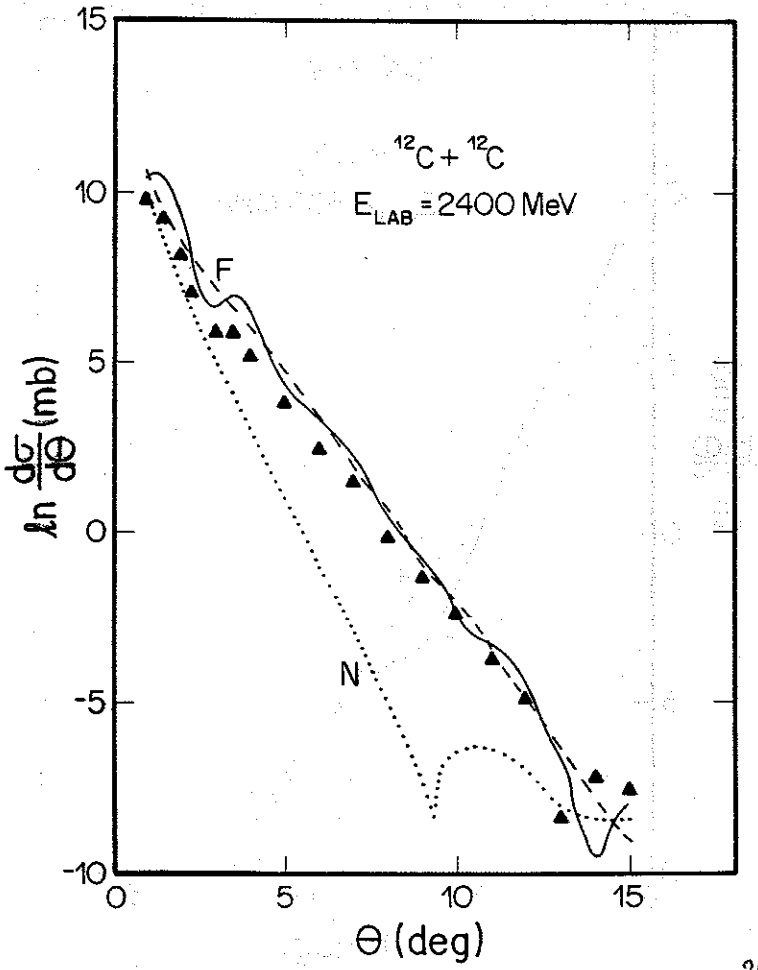
$^{12}C + ^{12}C$
$E_{LAB} = 2400$ MeV
F
N
$\ell n \frac{d\sigma}{d\Theta}$ (mb)
Θ (deg)
15
10
5
0
-5
-10
0
5
10
15

20

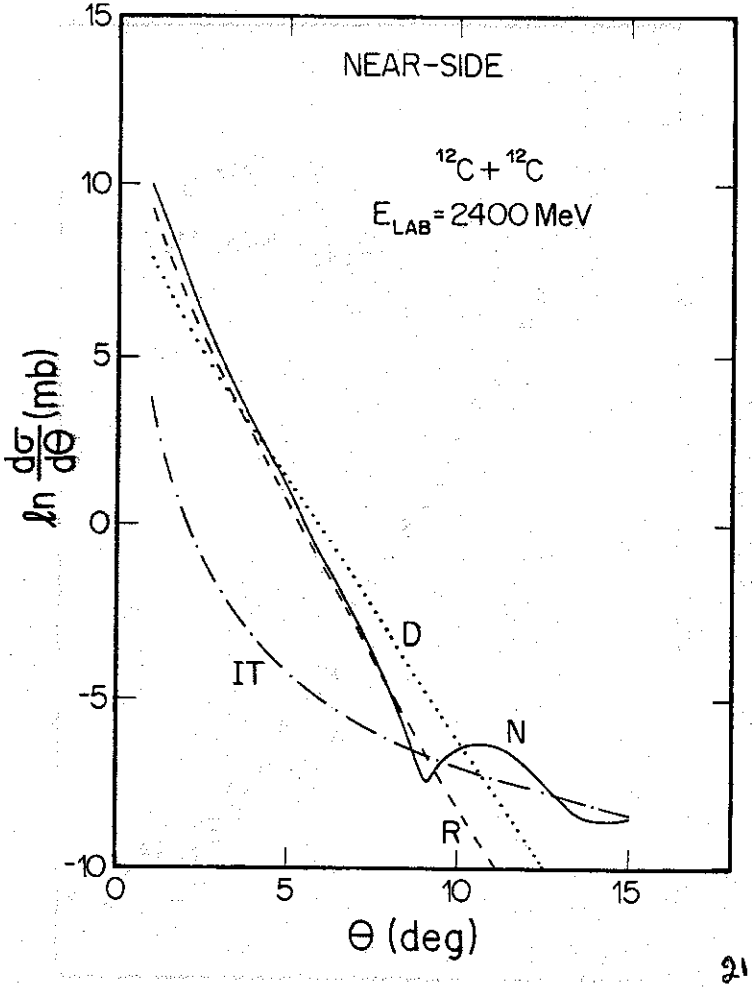
NEAR-SIDE
$^{12}C + ^{12}C$
E_{LAB} = 2400 MeV
$\ln \frac{d\sigma}{d\Theta}$ (mb)
Θ (deg)
D
IT
N
R
15
10
5
0
-5
-10
0
5
10
15

21

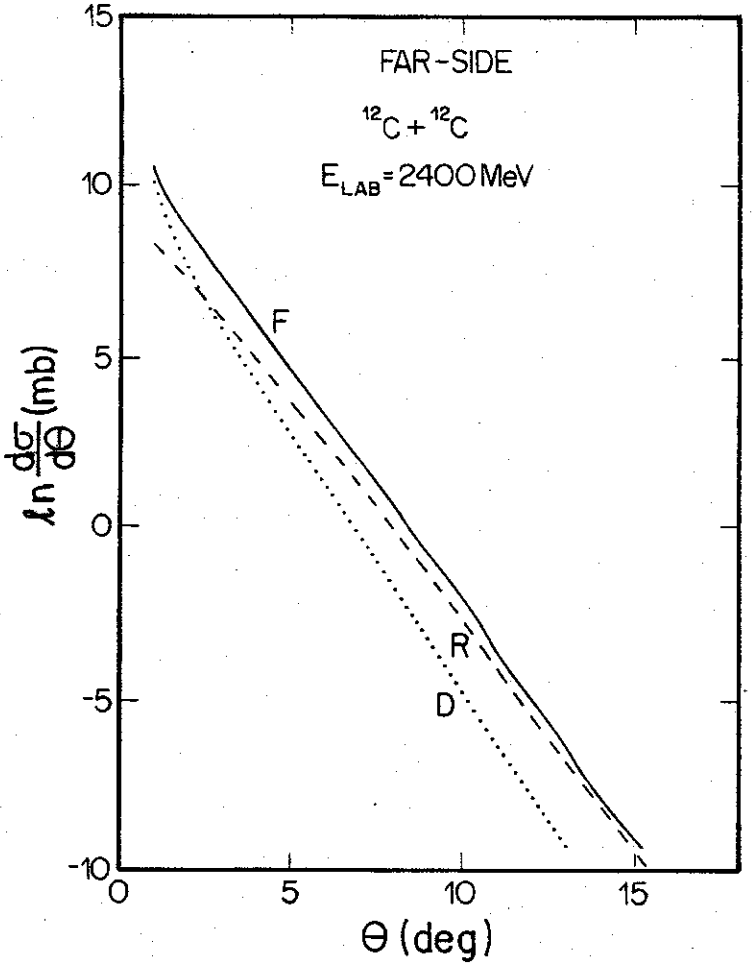
FAR-SIDE
$^{12}C + ^{12}C$
E_{LAB} = 2400 MeV
$\ln \frac{d\sigma}{d\Theta}$ (mb)
Θ (deg)
F
R
D
15
10
5
0
-5
-10
0
5
10
15

22

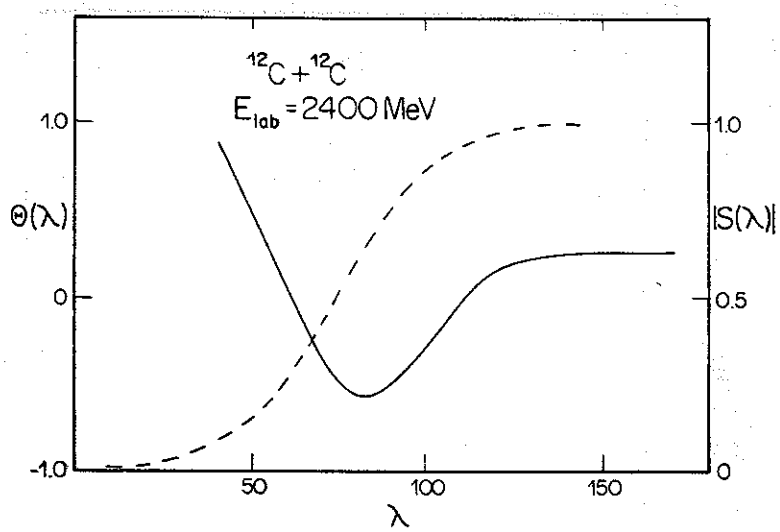
$^{12}C + ^{12}C$
$E_{lab} = 2400$ MeV
1.0
0
-1.0
Θ(λ)
|S(λ)|
1.0
0.5
0
50
100
150
λ

23

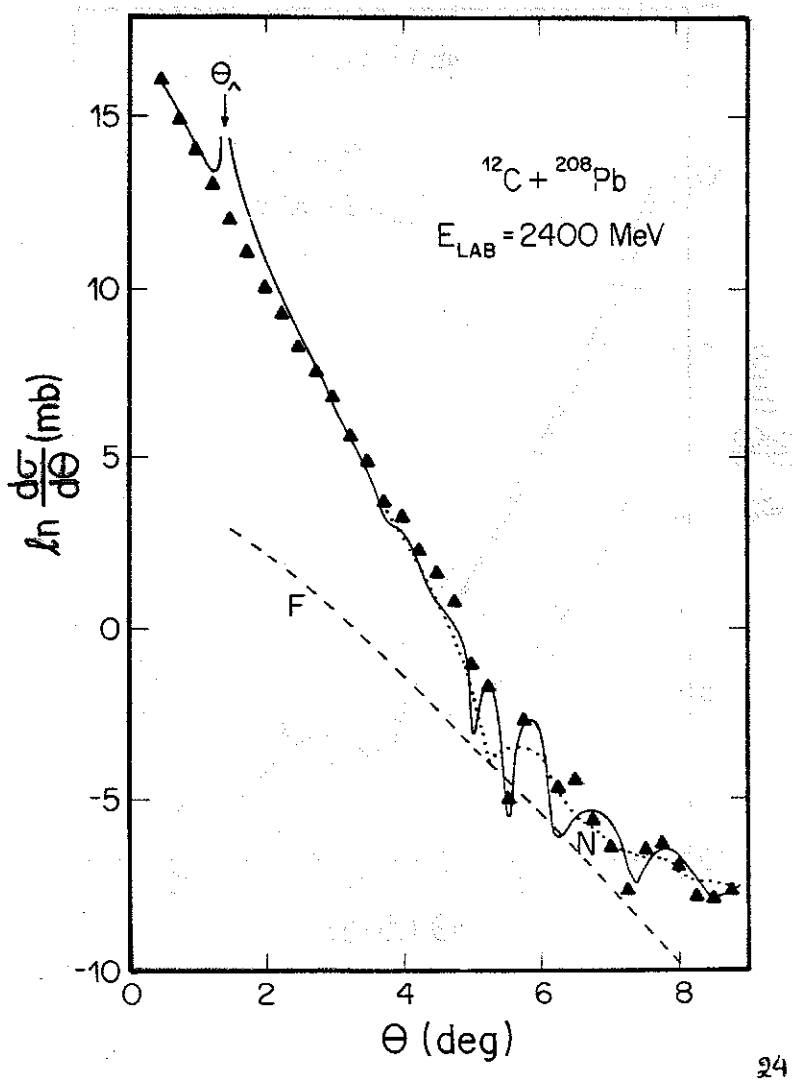
θ_r
$^{12}C + ^{208}Pb$
$E_{LAB} = 2400$ MeV
F
N
15
10
5
0
-5
-10
0
2
4
6
8
$\ln \frac{d\sigma}{d\Theta}$ (mb)
Θ (deg)

24

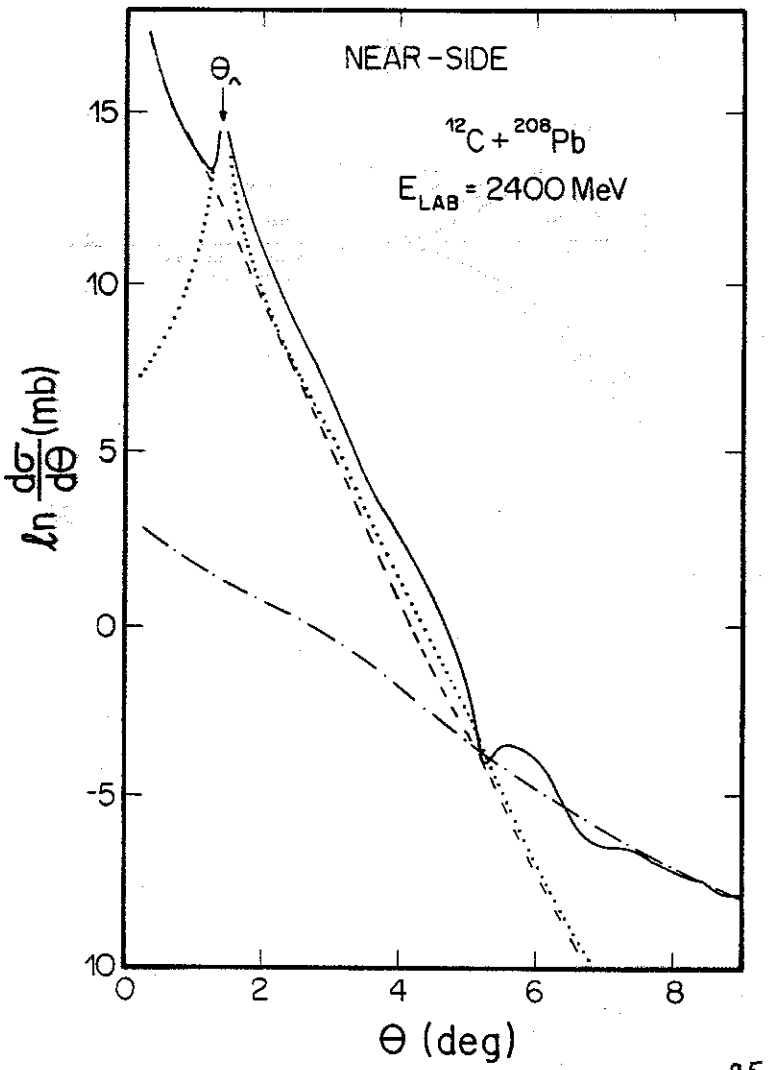
NEAR-SIDE
θ_r
$^{12}C + ^{208}Pb$
E_{LAB} = 2400 MeV
$\ln \frac{d\sigma}{d\theta}$(mb)
15
10
5
0
-5
10
0
2
4
6
8
θ (deg)

25

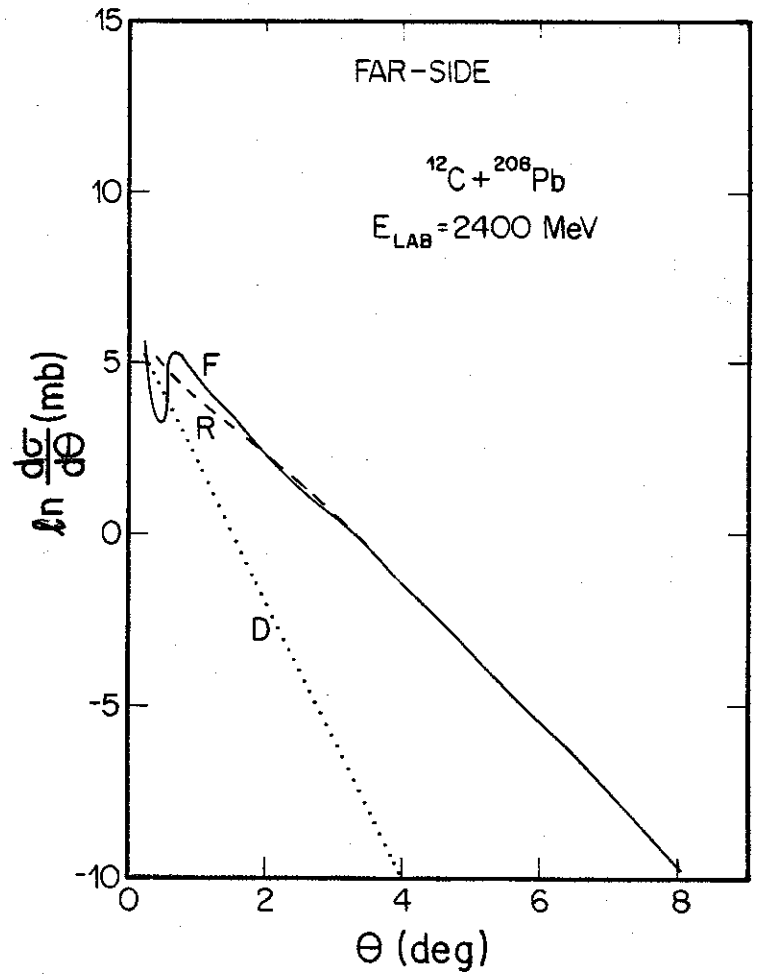
FAR-SIDE
$^{12}C + ^{208}Pb$
E_{LAB} = 2400 MeV
$\ln \frac{d\sigma}{d\theta}$(mb)
F
R
D
15
10
5
0
-5
-10
0
2
4
6
8
θ (deg)

26

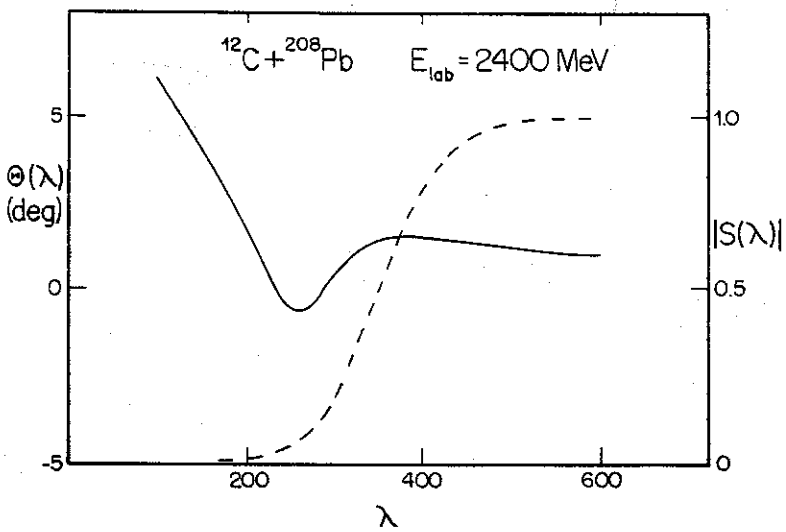
$^{12}C + ^{208}Pb$ $E_{lab} = 2400$ MeV
5
0
-5
Θ(λ) (deg)
1.0
0.5
0
|S(λ)|
200
400
600
λ

27

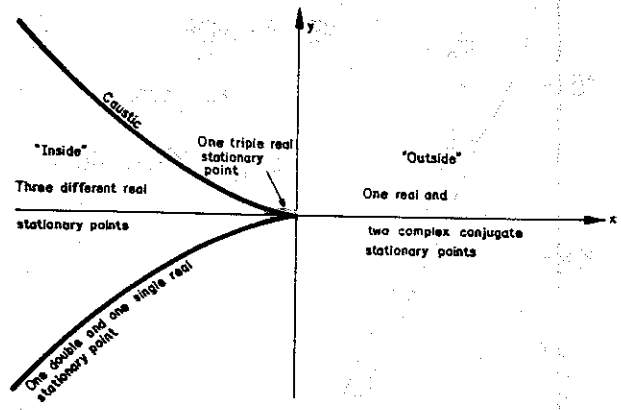
Caustic
"Inside"
Three different real stationary points
One triple real stationary point
"Outside"
One real and two complex conjugate stationary points
One double and one single real stationary point
y
x

28

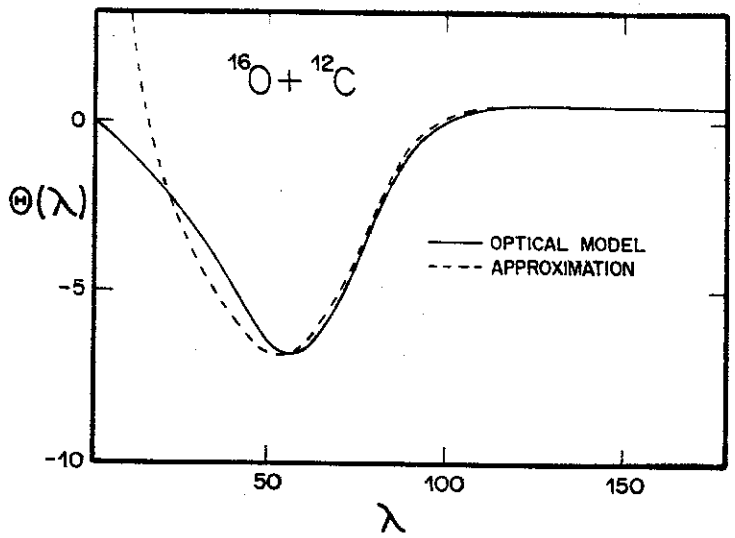
$^{16}O + ^{12}C$
0
-5
-10
Θ(λ)
50
100
150
λ
OPTICAL MODEL
APPROXIMATION

29

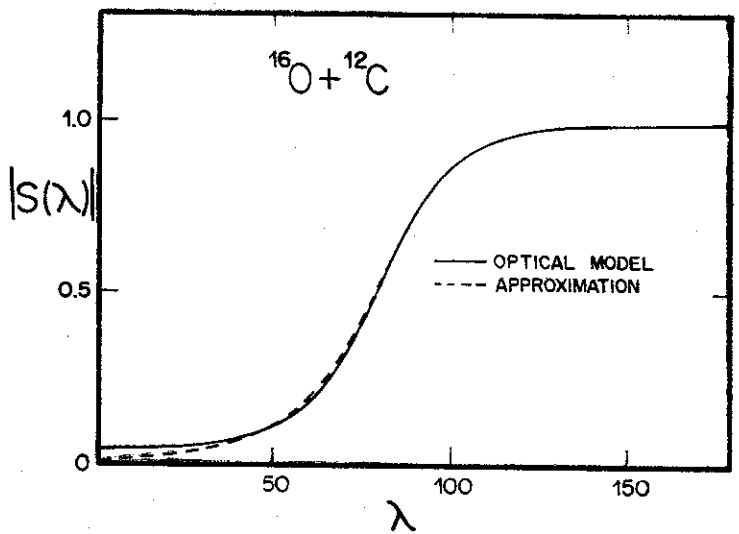
$^{16}O + ^{12}C$
1.0
0.5
0
|S(λ)|
50
100
150
λ
OPTICAL MODEL
APPROXIMATION

30